Defect flows in minimal models

Márton Kormos,[a,b,c] **Ingo Runkel**[a,1] **and Gérard M.T. Watts**[a]

[a]*Dept. of Mathematics, King's College London,*
Strand, London WC2R 2LS, U.K.

[b]*International School for Advanced Studies (SISSA),*
Via Beirut 4, 34014 Trieste, Italy

[c]*Istituto Nazionale di Fisica Nucleare, Sezione di Trieste,*
Via Beirut 2-4, 34131 Trieste, Italy

E-mail: kormos@sissa.it, Ingo.Runkel@kcl.ac.uk, Gerard.Watts@kcl.ac.uk

ABSTRACT: In this paper we study a simple example of a two-parameter space of renormalisation group flows of defects in Virasoro minimal models. We use a combination of exact results, perturbation theory and the truncated conformal space approach to search for fixed points and investigate their nature. For the Ising model, we confirm the recent results of Fendley et al. In the case of central charge close to one, we find six fixed points, five of which we can identify in terms of known defects and one of which we conjecture is a new non-trivial conformal defect. We also include several new results on exact properties of perturbed defects and on the renormalisation group in the truncated conformal space approach.

---

[1]E-mail from October 2010: Ingo.Runkel@uni-hamburg.de.

Contents

1 Introduction

By a defect in a two-dimensional conformal field theory we mean a line of inhomogeneity on the surface, where the expectation values of fields are allowed to be discontinuous or even singular. An example would be the continuum limit of a lattice model where the couplings are altered from their normal values along a line.

A typical defect is not invariant under a scale transformation and this leads to an action of the renormalisation group on the space of defects. The fixed points of the renormalisation group are clearly of interest and these are the conformal defects. The problem of studying conformal defects is equivalent to studying general conformal boundary conditions of a folded model [30]. Even if one starts from a rational conformal field theory, the folded model will typically no longer be rational with respect to the diagonal symmetry preserved by the boundary condition corresponding to the defect. This means that the representation theoretic methods used to construct the bulk theory cannot be applied to get a handle on the defect itself. There are, however, two distinguished subsets of conformal defects which are known as topological (or purely transmitting) defects and factorising (or purely reflecting defects), which are much easier to study than the general case.

Defects have an obvious generalisation to interfaces between different conformal field theories, possibly of different central charge. A particular model may, in fact, be simple enough to allow one to classify all conformal defects or interfaces; this is the case for defects in the Lee-Yang model [26] and in the critical Ising model [24], and for interfaces between the Lee-Yang and the Ising model [26]. Particular defects may preserve a rational sub-algebra in the folded model [12, 26, 27], or a semi-classical analysis may suggest the existence of distinguished conformal defects and interfaces, for example in a WZW model for a given group [5] or between such WZW models at different levels [14].

One may also think of interfaces as 'symmetries' which relate the properties of the two theories they link. For example, interfaces provide group symmetries and order-disorder dualities [16], they relate different renormalisation group flows of boundary conditions [22], there is a preferred interface joining the UV and IR fixed point of a given quantum field theory [7], and they can be used as spectrum generating symmetries in string theory [3]. Interfaces can also be related to tunnelling in the quantum Hall effect [11]. Defects (and also interfaces) can be composed by placing the defect lines parallel to each other and letting their distance tend to zero [4, 6, 17, 25, 29]. This process may or may not be singular, but if it can be defined then it describes an algebraic structure on the space of conformal field theories which deserves more investigation.

In this paper we study a very simple example of a two-parameter space of renormalisation group flows. We identify the fixed points of these flows with the aim of finding new non-trivial conformal defects. The starting point for our flows is a particular topological defect D in the Virasoro minimal model $M(p, p+1)$ and the two parameters of our space are λ_l and λ_r, describing perturbations of D. We arrive at the following conjecture for the space of flows for $p > 3$ in the neighbourhood of this defect, shown in figure 1. Note that, in this figure, λ_l and λ_r represent renormalised coupling constants. An example of such coupling constants are the coupling constants used in the TCSA scheme in section 5 taken at some fixed finite cut-off.
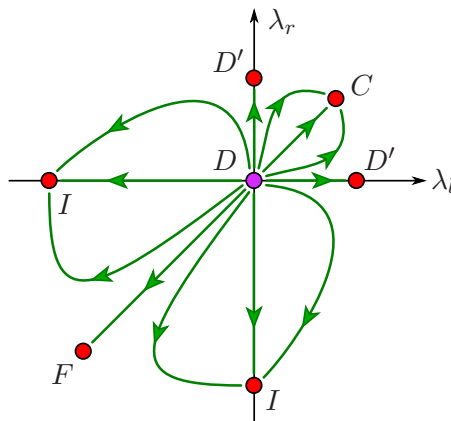
Figure 1. The proposed flows for the perturbation (2.23) for $p > 3$. The point D is the $(1, 2)$-defect. The possible endpoints are: I — the identity defect, D' — the $(2, 1)$-defect, F — a factorising defect given by the sum $\sum_{r=1}^{p-1} \| r, 1 \rangle\!\rangle \langle\!\langle r, 1 \|$ of $p-1$ conformal boundary conditions, and finally C — the new conformal defect. For details see the body of the paper.

Four of the fixed points (labelled D' and I) can be identified exactly and are topological defects; one can be studied numerically and we conjecture that it is a factorising defect F; finally we conjecture the existence of a new non-trivial conformal defect C which we study both numerically and perturbatively.

A renormalisation group analysis in the case of WZW models showed a similar non-trivial fixed point for $\lambda_l = \lambda_r \neq 0$, which is a good candidate for a non-topological conformal defect [5].

The case $p = 3$ has recently been studied in [11] and solved exactly by relating it to a free fermionic model. The space of RG flows is qualitatively different but the fixed points corresponding to I, C, D' and F are present in this model and agree with our conjectures for the exact forms of I, F and D'. Our numerical calculations agree with the results of [11], confirming the validity of our numerical method.

Unfortunately, we have so far been unable to calculate exactly or numerically other characteristic quantities of the new conformal defect C, such as its g-value [1] (defined to be that of the corresponding conformal boundary in the folded model) or its reflection coefficient [26]. However, we can calculate the g-value perturbatively for large values of p.

This paper is organised as follows. In section 2 we collect the properties of topological defects needed in the subsequent analysis. Section 3 contains several exact results on defects, some new to this paper. Section 4 contains the renormalisation group analysis of the perturbation for large p and identifies the new conformal defect as a perturbative fixed point. The numerial truncated conformal space approach used to support the proposed flows of figure 1 is described in section 5 with the results given in section 6. Finally, section 7 contains our conclusions.
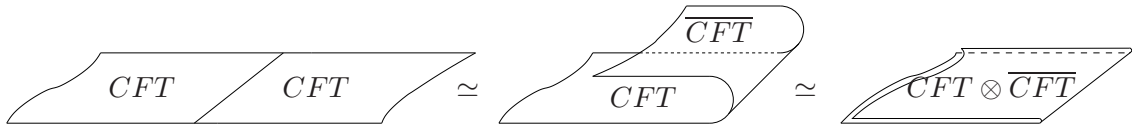
Figure 2. The equivalence between a defect in a CFT and a boundary condition in the folded model.

2 Topological, factorising and conformal defects

To derive the properties of conformal defects, consider the complex plane with a defect line placed on the real axis. The defect preserves the conformal symmetry of the bulk theory if the field $T_{xy} = \frac{i}{2\pi}(T - \bar{T})$ is continuous across the real axis.

This condition is unchanged if we now consider the defect on a cylinder obtained by identifying z with $z + 2\pi$. One can map this cylinder to the whole plane by $z \mapsto \exp(iz)$ and the real line gets mapped to the unit circle. In this formulation, a defect on the unit circle defines an operator D on the space of states $\mathcal{H}$ in radial quantisation. Translating the condition to this situation, a defect is conformal if the operator D commutes with the difference of the holomorphic and anti-holomorphic copy of the Virasoro modes,

$$[L_m - \bar{L}_{-m}, D] = 0 \quad \text{for all } m \in \mathbb{Z} . \tag{2.1}$$

General conformal defects of a given conformal field theory are difficult to describe because according to (2.1) they only preserve the diagonal Virasoro algebra $L_m^d = L_m - \bar{L}_{-m}$ (with central charge $c^d = c + \bar{c}$) of the full holomorphic and anti-holomorphic symmetry.

A very useful way to think of this condition is in terms of boundary conditions on the folded model. If one considers a CFT on the complex plane and folds the worldsheet over along the imaginary axis, the resulting model consists of the tensor product $CFT \otimes \overline{CFT}$ on the half plane with a boundary condition inserted along the imaginary axis as shown in figure 2, where $\overline{CFT}$ is the original CFT with holomorphic and anti-holomorphic dependences swapped. If the original model had a conformal defect along this line, (2.1) implies that it is a conformally invariant boundary condition in the folded model. Note that this includes the possibility that there is no defect (or the identity defect) so that there is a distinguished conformal boundary condition corresponding to the absence of any defect. This correspondence between defects in a CFT and boundary conditions on the folded model $CFT \otimes \overline{CFT}$ will often be used in what follows.

As said already, even if one starts from a rational model, the representation theoretic methods used to construct the bulk theory cannot be applied to get a handle on a general conformal defect. There are, however, two distinguished subsets of conformal defects which are much easier to study than the general case and which we consider now.

2.1 Topological defects and defect fields

Topological defects are a particular class of conformal defects which preserve a larger symmetry than the diagonal Virasoro symmetry and are amenable to classification on account of this. The larger symmetry in question is, in fact, the full bulk symmetry, that

is, the conformal defect obeys the stronger condition

$$[L_m, D] = 0 = [\bar{L}_m, D] \quad \text{for all } m \in \mathbb{Z}, \tag{2.2}$$

which clearly implies (2.1). Such defects are called topological because they are tensionless and can be deformed on the surface without affecting the value of correlators. Topological defects were first studied in [25] (and the name 'topological' was introduced in [5]). Condition (2.2) is equivalent to demanding that T and $\bar{T}$ are separately continuous across the defect line. As a consequence, the space of defect fields forms a representation of the holomorphic and anti-holomorphic copy of the Virasoro algebra, just as the space of bulk fields. In particular, a defect field ϕ has a left and right conformal weight (h_l, h_r).

The classification of topological defects can be carried out for rational conformal field theories and general modular invariants if one requires the defects to preserve the holomorphic and anti-holomorphic copy of the chiral algebra [18, 25]. Here we consider only the diagonal unitary Virasoro minimal models, for which the exposition simplifies.

Let thus $M(p, p+1)$ be the Virasoro minimal model of central charge $c = 1 - 6/(p^2 + p)$ and with diagonal modular invariant partition function. The irreducible representations R_i of the Virasoro algebra Vir occurring in these models are labelled by the set of Kac labels $i \in \mathcal{I}_p$,

$$\mathcal{I}_p = \big\{(r, s)\big| 1 \leq r \leq p-1, 1 \leq s \leq p\big\}/\sim \quad \text{where } (r, s) \sim (p-r, p+1-s) . \tag{2.3}$$

The space of states propagating on a cylinder, or equivalently the space of bulk fields, decomposes into representations of $\text{Vir} \oplus \overline{\text{Vir}}$ as

$$\mathcal{H} = \bigoplus_{i \in \mathcal{I}_p} R_i \otimes \bar{R}_i . \tag{2.4}$$

Both the elementary conformal boundary conditions [8] and the elementary topological defects [25] in $M(p, p+1)$ are labelled by the set $\mathcal{I}_p$. Let $\|a\rangle\rangle$ be the boundary state corresponding to removing the open unit disc from the complex plane and labelling the resulting boundary by $a \in \mathcal{I}_p$. Denote by $D_k : \mathcal{H} \to \mathcal{H}$ the operator describing a topological defect with label $k \in \mathcal{I}_p$ placed on the unit circle in the complex plane. Explicitly, these two quantities are given by

$$\|a\rangle\rangle = \sum_{i \in \mathcal{I}_p} \frac{S_{ai}}{\sqrt{S_{0i}}} |i\rangle\rangle \quad \text{and} \quad D_k = \sum_{i \in \mathcal{I}_p} \frac{S_{ki}}{S_{0i}} id_{R_i \otimes \bar{R}_i} , \tag{2.5}$$

where 0 is the identity or vacuum representation $(1, 1)$, $|i\rangle\rangle$ is the Ishibashi state in the (algebraic completion of) $R_i \otimes \bar{R}_i$ and S_{ij} is the modular S-matrix for $M(p, p+1)$,

$$S_{(r,s)\,(x,y)} = \sqrt{8/(p^2 + p)} \cdot (-1)^{1+sx+ry} \cdot \sin \frac{\pi(p+1)rx}{p} \cdot \sin \frac{\pi p s y}{p+1} . \tag{2.6}$$

An important property of a defect is its entropy g defined in the same way as the boundary entropy and identical in value to the boundary entropy of the corresponding boundary

condition in the folded model [1]. From (2.5) we read off the g-value of a boundary condition and a topological defect as

$$g(\,\|a\rangle\!\rangle) = \frac{S_{a0}}{\sqrt{S_{00}}} \quad \text{and} \quad g(D_k) = \frac{S_{k0}}{S_{00}} \;. \tag{2.7}$$

We recall that topological defects can be deformed freely on the surface as long as they do not cross field insertions, boundaries, or defect lines. The fusion of two topological defects corresponds to the composition of the defect operators, and the fusion of a defect with a boundary condition is given by the action of the defect operator on the boundary state. One easily checks that for $i, j, k, a \in \mathcal{I}_p$,

$$D_{(1,1)} = id_{\mathcal{H}} \;, \quad D_k \, D_l = \sum_{m \in \mathcal{I}_p} N_{kl}{}^m \, D_m \;, \quad D_k \, \|a\rangle\!\rangle = \sum_{b \in \mathcal{I}_p} N_{ka}{}^b \, \|b\rangle\!\rangle \;, \tag{2.8}$$

where $N_{ij}{}^k$ are the fusion rule coefficients. By evaluating the corresponding partition functions, or by using the methods of [17], one finds that the space of defect fields living on a defect labelled by $k \in \mathcal{I}_p$ is given by

$$\mathcal{H}_k^D = \bigoplus_{i,j \in \mathcal{I}_p} \left(R_i \otimes \bar{R}_j \right)^{\oplus \sum_{x \in \mathcal{I}_p} N_{ij}{}^x N_{kk}{}^x} \;. \tag{2.9}$$

We will also need the space of states propagating on a strip with boundary condition $(1, 1)$ on one side and $a \in \mathcal{I}_p$ on the other side, and with a defect labelled $k \in \mathcal{I}_p$ running parallel to the boundaries inside the strip. In the same way as (2.9) one finds this is

$$\mathcal{H}_k^{(1,1),a} = \bigoplus_{i \in \mathcal{I}_p} R_i^{\oplus N_{ak}{}^i} \;. \tag{2.10}$$

2.2 Factorising defects

By a factorising defect we mean a conformal defect represented by an operator F that satisfies the stronger conditions

$$(L_m - \bar{L}_{-m})F = 0 = F(L_m - \bar{L}_{-m}) \quad \text{for all } m \in \mathbb{Z} \,, \tag{2.11}$$

which then imply (2.1). Such a defect is totally reflecting and is simply a sum of products of conformal boundary states

$$F = \sum_{a,b \in \mathcal{I}_p} n_{ab} \, \|a\rangle\!\rangle \, \langle\!\langle b\| \tag{2.12}$$

for some non-negative integers n_{ab}. In the folded model this corresponds to separate boundary conditions on the two sheets, as in figure 3. The g-value of the factorising defect (2.12) is

$$g(F) = \sum_{a,b \in \mathcal{I}_p} n_{ab} \frac{S_{a0} S_{b0}}{S_{00}} \;. \tag{2.13}$$

Figure 3. The equivalence between a factorising defect in a CFT and separate boundary conditions in the folded model.

2.3 Conformal defects

Returning to general conformal defects, we give the form of the partition function on a cylinder and define a useful pairing on such defects.

Let d and d' label two conformal defects and consider a torus of width R and height L with two vertical defect lines at distance ηR, $0 < \eta < 1$, from each other. Denote by D_d and $D_{d'}$ the defect operators of the defects d and d'. Define the partition function

$$Z_{d,d'}(q;\eta) = \text{tr}_{\mathcal{H}}\Big(\tilde{q}^{\,\eta(L_0+\bar{L}_0-c/12)}\,(D_d)^\dagger\,\tilde{q}^{\,(1-\eta)(L_0+\bar{L}_0-c/12)}\,D_{d'} \Big) \tag{2.14}$$

where $q = e^{-2\pi L/R}$ and $\tilde{q} = e^{-2\pi R/L}$. The adjoint $(D_d)^\dagger$ describes the defect operator for the defect d inserted with reversed orientation (see [25] and [19, sect. 6.1]). Using the explicit expressions (2.5) one checks that for the factorising and topological defects in $M(p, p+1)$ one has

$$(\|a\rangle\!\rangle\langle\!\langle b\|)^\dagger = \|b\rangle\!\rangle\langle\!\langle a\| \quad\text{and}\quad (D_k)^\dagger = D_k \,. \tag{2.15}$$

In the special case that $\eta = \frac{1}{2}$, we can identify the original CFT on a torus with two defects with the folded model on a cylinder of circumference L and width $R/2$ with conformal boundary conditions corresponding to the defects d and d' at the ends of the cylinder. The partition function of the folded model on a cylinder of circumference L and width $R/2$ is a sum of Virasoro characters $\chi_{h,2c}(q)$ at twice the central charge of $M(p, p+1)$, so that the partition function can be written as

$$Z_{d,d'}\left(q;\frac{1}{2}\right) = \sum_h m_h\,\chi_{h,2c}(q) \tag{2.16}$$

where $q = e^{-2\pi L/R}$, m_h is the multiplicity of the representation with highest weight h and the sum can be over a finite or infinite set of weights h. We have assumed that the spectrum of the folded model on the strip is discrete, i.e. that $Z_{d,d'}(q;\frac{1}{2})$ is a sum of powers of q, rather than an integral. This may not be the case for a general conformal defect, but it is true for the topological defects D_k and for the totally factorising defects $\|a\rangle\!\rangle\langle\!\langle b\|$ as can be checked with the explicit expression in (2.5). We investigate defects which can be reached by renormalisation group flows starting at these defects, and so we expect the spectrum at the IR fixed point to be discrete as well.

We define the pairing (d, d') by

$$(d, d') = m_0 \in \mathbb{Z}_{\geq 0}\,, \tag{2.17}$$

i.e. the multiplicity of the vacuum character in $Z_{d,d'}(q;\frac{1}{2})$. For unitary models conformal weights have to be non-negative so that we can write (d, d') as the limit

$$(d, d') = \lim_{q\to 0} q^{c/12}\,Z_{d,d'}\left(q;\frac{1}{2}\right)\,. \tag{2.18}$$

Since $\text{tr}(X) = (\text{tr}(X^\dagger))^*$ for any operator X, and (d, d') is real, it follows from (2.18) that $(d, d') = (d', d)$.

By passing to the folded model one checks that $(d, d) \geq 1$, that $(d, d) = 1$ if and only if the conformal defect d is elementary, and that $(d, d') = 0$ if d and d' are elementary and distinct. The latter statement follows in the folded model since one cannot have a boundary changing field of weight zero between two distinct elementary boundary conditions a and b (such a field could be pushed along the a boundary changing it into a b boundary without affecting correlators, showing that a and b have equal boundary states[1]).

In particular, if d is a superposition and d' is elementary, then (d, d') gives the multiplicity of d' in the decomposition of d into elementary defects.

Another useful property of the pairing is that if $k \in \mathcal{I}_p$ is a topological defect, and $k \star d$ denotes the fused defect (which is again conformal and has the defect operator $D_k D_d$) we have

$$(k \star d, d') = (d, k \star d') \quad \text{and} \quad (d \star k, d') = (d, d' \star k) \,. \tag{2.19}$$

The first equality follows from

$$\text{tr}_{\mathcal{H}} \Big(\tilde{q}^{\frac{1}{2}(L_0 + \bar{L}_0 - c/12)} (D_k D_d)^\dagger \, \tilde{q}^{\frac{1}{2}(L_0 + \bar{L}_0 - c/12)} \, D_{d'} \Big) \tag{2.20}$$
$$= \text{tr}_{\mathcal{H}} \Big(\tilde{q}^{\frac{1}{2}(L_0 + \bar{L}_0 - c/12)} (D_d)^\dagger \, \tilde{q}^{\frac{1}{2}(L_0 + \bar{L}_0 - c/12)} \, D_k D_{d'} \Big)$$

as D_k is self-adjoint and commutes with $L_0 + \bar{L}_0$. The second equality can be seen similarly.

2.4 Defect perturbations

Finally we consider perturbations of topological defects. A perturbation of a topological defect by a defect field ϕ_{h_l, h_r} is relevant if $h_l + h_r < 1$. This is in contrast to bulk perturbations, which are integrated over the whole surface, not just over the defect line, and are relevant if $h_l + h_r < 2$.

The first thing to note is that all topological defects in unitary minimal models have relevant perturbations, even the identity defect (that is, no defect), which is quite different from the boundary situation where there are $(p-1)$ stable boundary conditions for $M(p, p+1)$. The fields on the identity defect are all scalars and are exactly the bulk fields $\phi_{h,h}$. There are $\lfloor \sqrt{2p^2 + 2p + 1} \rfloor - 2$ of these with scale dimension less than or equal to 1, as opposed to $2p - 3$ which have scale dimension ≤ 2. In any case, even the identity defect is unstable to defect perturbations by these bulk fields (considered as fields on the defect).

As another example, on the $(1, 2)$ defect there are both scalar primary fields $\phi_{h,h}$ and non-scalar primary fields $\phi_{h,h'}$ with $h \neq h'$. There are $(p-1)^2$ scalar primary fields of which $2\lfloor \sqrt{2p^2 + 2p + 1} \rfloor - 6$ have dimension ≤ 1 and $(p-1)(p-2)$ non-scalar primary fields of which $2(p-2)$ have dimension ≤ 1. The relevant non-scalar fields are

$$\{\phi_{(r,r),(r,r+2)} \text{ and } \phi_{(r,r+2),(r,r)} \mid 1 \leq r \leq p - 2\} \,. \tag{2.21}$$

---

[1]Some care has to be taken since in general the boundary state does not characterise the boundary condition uniquely. Similarly, the defect operator does in general not determine the defect uniquely. An example of this is discussed in [19]. For unitary models this ambiguity is not expected to occur, i.e. there is a one-to-one correspondence between boundary conditions and boundary states, and similar for defects.

We note here that the interpretation of a defect as a boundary condition in a folded model means that the boundary g-theorem [1, 15] applies to perturbed defects as well: g is decreasing along RG flows and so restricts the possible IR fixed points accessible from any given UV fixed point.

The simplest class of relevant perturbations are those by chiral defect fields $\phi_{h,0}$ or $\phi_{0,h}$ with $h < 1$. Such perturbations were investigated in [29]. These perturbed defects are believed to have particularly nice properties, for example to commute with $L_0 + \bar{L}_0$, see section 2.4.1 below.

On the other hand, since a topological defect perturbed by $\lambda_l \cdot \phi_{h,0}$, say, will commute with all $\bar{L}_m$ for arbitrary values of the coupling λ_l, the conformal defect obtained as the IR fixed point for large λ_l will necessarily be topological [5]. To obtain an IR fixed point which is conformal but not topological, the next simplest perturbation to try is the defect field

$$\lambda_l \cdot \phi_{h,0} \ + \ \lambda_r \cdot \phi_{0,h} \ . \tag{2.22}$$

A topological defect perturbed by this field will no longer commute with either the L_m's or the $\bar{L}_m$'s and in general it will also not commute with $L_0 + \bar{L}_0$ (there are exceptions, for example the fusion of a defect perturbed by $\phi_{h,0}$ with a defect perturbed by $\phi_{0,h}$).

For the conformal weight h in (2.22) we choose $h_{(1,3)} = (p - 1)/(p + 1)$. This field is of interest for several related reasons: in many circumstances it leads to integrable perturbations which can be solved exactly and we expect the purely chiral perturbations to be integrable and exactly solvable; this perturbation is also related to one of the integrable lattice description of minimal models; finally, it is particularly suitable for a renormalisation group analysis, as it does not generate further relevant fields under fusion (note that $\phi_{h,h}$ already has weight greater than or equal to 1), and it becomes marginal in the limit $p \to \infty$.

The simplest topological defect which allows for a perturbation by (2.22) is the $(1, 2)$-defect, and so this is finally the situation which we will study:

$$D_{12}(\lambda_l \phi + \lambda_r \bar{\phi}) \tag{2.23}$$

The (1,2)-defect perturbed by $\lambda_l \phi + \lambda_r \bar{\phi}$ with $\phi = \phi_{h_{(1,3)},0}$ and $\bar{\phi} = \phi_{0,h_{(1,3)}}$.

There are two useful results which we can derive for this perturbed defect which we give now.

2.4.1 Translation invariance

As mentioned above, it is believed that a topological defect perturbed by a chiral field still commutes with $L_0 + \bar{L}_0$. This is shown in [29] for chiral fields with $h < 1/2$ where there are no UV divergences in the expansion of the perturbed defect; for fields with $h \geq 1/2$ this property depends on the existence of a suitable regulator which preserves the commutators. Assuming for the moment that such a regulator can be found, in the present case this would imply

$$[L_0 + \bar{L}_0, D_{(1,2)}(\lambda\phi)] = 0 \quad \text{and} \quad [L_0 + \bar{L}_0, D_{(1,2)}(\lambda\bar{\phi})] = 0 \ . \tag{2.24}$$

This guarantees that the action of $D_{(1,2)}(\lambda\phi)$ and $D_{(1,2)}(\lambda\bar{\phi})$ on a boundary state is non-singular.

One particular consequence of the property (2.24) is that the spectrum of states of the model on a strip containing a defect parallel to the edges of the strip is independent of the position of the defect. This is easy to see in the case of the TCSA regulator, as we prove in appendix D, so that it is very reasonable to apply this assumption to our TCSA results and we will use this in section 3.1 to deduce the end-points of the chiral perturbations.

2.4.2 Commutation with a subset of topological defects

Let $D(\sum_\alpha \lambda_\alpha \phi_\alpha)$ be a topological defect perturbed by defect fields ϕ_α where ϕ_α is a field (not necessarily primary) in the sector $R_{k_\alpha} \otimes \bar{R}_{l_\alpha}$. Suppose that either all of the k_α are of the form $(1, s_\alpha)$ with s_α odd, or all of the l_α are of the form $(1, s_\alpha)$ with s_α odd. Then

$$\left[D_{(r,1)} , D(\textstyle\sum_\alpha \lambda_\alpha \phi_\alpha) \right] = 0 \quad \text{for } 1 \le r \le p-1 . \tag{2.25}$$

We will demonstrate this in the case that the k_α are of the form $(1, s_\alpha)$ with s_α odd. The second case can be seen analogously.

Let $x \in R_i \otimes \bar{R}_i$ and $y \in R_j \otimes \bar{R}_j$ for $i = (a,b)$ and $j = (c,d)$ elements of $\mathcal{I}_p$. From the explicit form of $D_{(r,1)}$ in (2.5) and abbreviating $D \equiv D(\sum_\alpha \lambda_\alpha \phi_\alpha)$ we find

$$\langle x | D_{(r,1)} D | y \rangle = \frac{S_{(r,1)(a,b)}}{S_{(1,1)(a,b)}} \langle x | D | y \rangle , \quad \langle x | D D_{(r,1)} | y \rangle = \frac{S_{(r,1)(c,d)}}{S_{(1,1)(c,d)}} \langle x | D | y \rangle . \tag{2.26}$$

Now expand out the exponential in $\langle x | D | y \rangle$. Since each term in the integrand is in the sector $R_{(1,s_\alpha)} \otimes \bar{R}_{l_\alpha}$, the expression $\langle x | D | y \rangle$ can be non-zero only if i and j are such that $a=c$ and $b-d$ is even. Substituting the expression (2.6) for S_{ij} gives

$$\frac{S_{(r,1)(a,b)}}{S_{(1,1)(a,b)}} = (-1)^{(r+1)b} \frac{\sin(\pi(p+1)ra/p)}{\sin(\pi(p+1)a/p))} . \tag{2.27}$$

Since $a=c$ and $b-d$ is even, the two expressions in (2.26) are therefore equal for all states x, y, proving (2.25).

For us the commutator (2.25) is interesting because it implies $[D_{(r,1)}, D_{(1,2)}(\lambda_l \phi + \lambda_r \bar{\phi})] = 0$ with ϕ and $\bar{\phi}$ as in (2.23). However, let us note in passing that (2.25) can also be applied to bulk perturbations. In particular, we can set $D = \exp(-\ell H)$ with H the Hamiltonian of the minimal model perturbed by the bulk field $\phi_{(1,3),(1,3)}$ since

$$H = \int \left(\frac{1}{2\pi}(T+\bar{T}) + \mu \phi_{(1,3),(1,3)} \right) \, \mathrm{d}x \tag{2.28}$$

and T and $\bar{T}$ are descendent fields in the $(1,1)$ representation. The topological defects $D_{(r,1)}$ continue to commute with D for all values of the coupling μ, and thus they are conserved charges also off criticality. This provides an independent argument for the observation made in [13] that under the bulk flow between two minimal models generated by $\phi_{(1,3),(1,3)}$, the topological defect $D_{(r,1)}$ should again flow to a topological defect.

3 Exact results

The properties (2.24) and (2.25) of $D_{(1,2)}(\lambda_l\phi + \lambda_r\bar\phi)$ enable us to find two exact results for the perturbed defect, which we describe in sections 3.1 and 3.2. We also summarise in section 3.3 the known results for the Ising model (the case $p = 3$) which is distinct from the other models.

3.1 The chiral perturbations

The translation invariance of the purely chiral and purely anti-chiral perturbations in (2.24) allows us to determine the nature of these flows exactly.

Consider the situation described in (2.23), i.e. $D_{(1,2)}(\lambda_l\phi + \lambda_r\bar\phi)$ is the operator obtained by placing the $(1, 2)$-defect on the unit circle and perturbing by $\lambda_l\phi + \lambda_r\bar\phi$ with λ_l and $\lambda_r \in \mathbb{R}$. Let ψ be the primary boundary field on the $(1, 2)$-boundary condition in the $R_{(1,3)}$ representation and denote by $\|(1, 2) + \lambda\psi\rangle\!\rangle$ the boundary state obtained by perturbing the $(1, 2)$-boundary by $\lambda\psi$. One can normalise the fields ϕ, $\bar\phi$ and ψ such that the identity[2]

$$D_{(1,2)}(\lambda\phi)\|1,1\rangle\!\rangle = \|(1, 2) + \lambda\psi\rangle\!\rangle = D_{(1,2)}(\lambda\bar\phi)\|1,1\rangle\!\rangle \tag{3.1}$$

holds. The boundary flows in the middle of this series of equalities are already known [21, 23, 28],

$$\|1,1\rangle\!\rangle \xleftarrow{\;-\infty\leftarrow\lambda\;} \|(1, 2) + \lambda\psi\rangle\!\rangle \xrightarrow{\;\lambda\to+\infty\;} \|2,1\rangle\!\rangle \, . \tag{3.2}$$

As mentioned in section 2.4, a chirally perturbed topological defect necessarily has again a topological defect as an IR fixed point. Acting with the IR topological defect on $\|1,1\rangle\!\rangle$ gives a conformal boundary state that has to agree with (3.2). The explicit expressions in (2.5) show that a topological defect is uniquely determined by its action on $\|1,1\rangle\!\rangle$, so that the above reasoning fixes the horizontal and vertical flows in figure 1 to be

$$
\begin{aligned}
I \equiv D_{(1,1)} &\quad \xleftarrow{\;-\infty\leftarrow\lambda_l\;} \quad D_{(1,2)}(\lambda_l\phi) \quad \xrightarrow{\;\lambda_l\to+\infty\;} \quad D' \equiv D_{(2,1)} \, , \\
I \equiv D_{(1,1)} &\quad \xleftarrow{\;-\infty\leftarrow\lambda_r\;} \quad D_{(1,2)}(\lambda_r\bar\phi) \quad \xrightarrow{\;\lambda_r\to+\infty\;} \quad D' \equiv D_{(2,1)} \, .
\end{aligned}
\tag{3.3}
$$

3.2 The factorising component of any IR fixed point

The fact that our perturbed defects commute with the set of topological defects $\{D_{(t,1)}\}$ shown in (2.25) allows us to determine the building blocks of any factorising component of any IR fixed point.

Consider the superposition of elementary factorising defects given by

$$F^{s|s'} = \sum_{t=1}^{p-1} D_{(t,1)}\|1, s\rangle\!\rangle\langle\!\langle 1, s'\|D_{(t,1)} \cdot \begin{cases} \frac{1}{2} & : p \text{ odd and } s = s' = \frac{p+1}{2} \\ 1 & : \text{otherwise} \end{cases} \, . \tag{3.4}$$

---

[2]This identity is evident in the case $\lambda = 0$. Since the space of $(1, 3)$-primary fields on the $(1, 2)$-boundary is one-dimensional and spanned by ψ, the perturbing fields ϕ and $\bar\phi$ have to be proportional to ψ once the $(1, 2)$-defect is pushed on top of the $(1, 1)$-boundary. Alternatively, the identity can be proved with the methods in [17].

The factor of $\frac{1}{2}$ has to be included because for $s = s' = \frac{p+1}{2}$ we have $\|t, \frac{p+1}{2}\rangle\!\rangle\langle\!\langle t, \frac{p+1}{2}\| = \|p - t, \frac{p+1}{2}\rangle\!\rangle\langle\!\langle p - t, \frac{p+1}{2}\|$, so that in this case each factorising defect appears twice in the sum. For example, in the Ising model ($p = 3$) we have $F^{2|2} = \|1, 2\rangle\!\rangle\langle\!\langle 1, 2\|$.

It is shown in appendix A that $[D_{(r,1)}, F^{s|s'}] = 0$ for $r = 1, \ldots, p-1$, and that the following statement is true: If a conformal defect C obeys $[D_{(2,1)}, C] = 0$ (which implies that $[D_{(r,1)}, C] = 0$ for all r) then we can write

$$C = R + F \tag{3.5}$$

where R is a conformal defect that does not contain factorising defects as summands, i.e. $(R, \|a\rangle\!\rangle\langle\!\langle b\|) = 0$ for all $a, b \in \mathcal{I}_p$, and where F is a combination of factorising defects taking the form

$$F = \sum_{s,s'=1}^{p} \sum_{a=1}^{p-1} m_a^{s|s'} D_{(a,1)} F^{s|s'} \tag{3.6}$$

for suitable constants $m_a^{s|s'} \in \mathbb{Z}_{\geq 0}$. If C is an IR fixed point of $D_{(1,2)}(\lambda_l \phi + \lambda_r \bar{\phi})$ in a particular direction in the (λ_l, λ_r)-plane, it will commute with the $D_{(r,1)}$ and hence can be written in the form (3.5). This will be exploited in the g-function analysis in section 4 and in identifying the spectrum on a strip with a perturbed defect via TCSA in section 6.

3.3 The Ising case

The Ising model is unique amongst unitary minimal models in that its conformal defects can be completely classified. The reason is that its square Ising⊗Ising is a $c = 1$ CFT which can be described in terms of an orbifolded free boson. Using this relation, Oshikawa and Affleck give a complete classification in [24] of the conformal defects of the Ising model in terms of the conformal boundary conditions of the orbifolded boson as follows.

There is a continuous family of Dirichlet boundary conditions $D(\varphi_0)$ subject to $D(\varphi_0) = D(-\varphi_0) = D(\varphi_0 + 2\pi)$ for which a fundamental domain is $\varphi_0 \in [0, \pi]$; and a continuous family of Neumann boundary conditions $N(\tilde{\varphi}_0)$ with $N(\tilde{\varphi}_0) = N(-\tilde{\varphi}_0) = N(\tilde{\varphi}_0 + \pi)$ for which a fundamental domain is $\tilde{\varphi} \in [0, \frac{\pi}{2}]$. The boundary conditions in the two continuous families are all elementary, except for the boundary conditions at the endpoints of the fundamental domains, which each split into two elementary boundary conditions so giving a discrete set of eight boundary conditions. Altogether we have

$$|D(\varphi_0)\rangle \quad \text{with } \varphi_0 \in (0, \pi) \qquad \text{and } |D(0)\rangle_\pm, \ |D(\pi)\rangle_\pm,$$
$$|N(\tilde{\varphi}_0)\rangle \quad \text{with } \tilde{\varphi}_0 \in (0, \pi/2) \quad \text{and } |N(0)\rangle_\pm, \ |N(\pi/2)\rangle_\pm.$$

These have g values $\sqrt{2}$ for the continuous Neumann series, 1 for the continuous Dirichlet series, $1/\sqrt{2}$ for the discrete Neumann defects and $1/2$ for the discrete Dirichlet defects.

There are three topological defects in the Ising model given by Kac labels $(1, 1) = \text{id}$, $(1, 2) = \sigma$ and $(2, 1) = \varepsilon$ and three Cardy boundary conditions "$+$" $= (1, 1)$, "f" $= (1, 2)$ and "$-$" $= (2, 1)$. The topological and factorising defects are identified with the orbifolded boson boundary conditions [24, 26] as shown in figure 4.
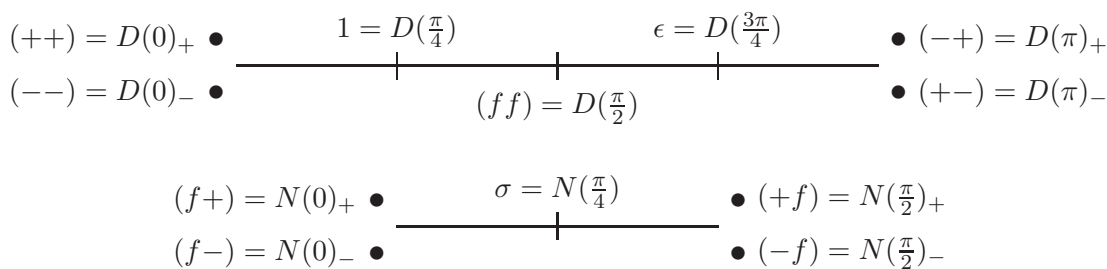
Figure 4. The Dirichlet (top) and Neumann (bottom) boundary conditions on the orbifolded free boson and the corresponding topological and factorising defects in the folded Ising model.

To identify the fixed points of the numerical RG flows in section 6.1 we need the partition function encoding the spectrum of states on a strip with the $(1,1) = $"+" boundary condition on the two edges and a defect in the middle. When this strip is folded, this is equal to the partition function in the orbifolded boson model with the $(++) = D(0)_+$ boundary condition at one side of the folded strip and some boundary condition corresponding to the Ising defect at the other boundary. In the UV this is the $(1,2) = \sigma = N(\pi/4)$ boundary condition, but by the g-theorem, the IR point fixed point can be any Dirichlet boundary condition (together with any of the four discrete Neumann conditions, but these do not arise in the flows we consider); the partition function of such a system is given in [24]

$$
Z_{D(0)_+, D(\varphi_0)}\left(q; \frac{1}{2}\right) = \frac{q^{\frac{1}{2}(\frac{\varphi_0}{\pi})^2}}{\eta(q)} \sum_{n=-\infty}^{\infty} q^{2n^2 + 2n\frac{\varphi_0}{\pi}} \, , \tag{3.7}
$$

where $q = e^{-2\pi L/R}$. This expression is also valid at the endpoints $\varphi_0 = 0, \pi$ if one takes $D(0) = D(0)_+ + D(0)_-$ and $D(\pi) = D(\pi)_+ + D(\pi)_-$.

As has been discussed in section 3.1, the IR fixed points of the purely chiral flows can be easily found: they are the $(2,1) = \varepsilon$ and $(1,1) = \mathrm{id}$ topological defects in the positive and negative directions, respectively. The remaining fixed points have been recently found (amongst other results) in [11] and the space of flows is shown in figure 13(a). In that paper, the perturbed defects are parametrised by an angle θ with the general result

$$
N(\tilde{\varphi}_0) \ \longrightarrow \ D(\tilde{\varphi}_0 + \theta) \, . \tag{3.8}
$$

We define the angle α by $\tan(\alpha) = \lambda_r/\lambda_l$, with $\alpha \in (-\frac{\pi}{2}, \frac{\pi}{2})$ for $\lambda_l > 0$ and $\alpha \in (\frac{\pi}{2}, \frac{3\pi}{2})$ for $\lambda_l < 0$. One can check that α is related to θ by $\alpha = \pi - \theta$ so that the prediction of [11] for the RG flows of the defects (2.23) is

$$
D_\sigma = N(\pi/4) \ \longrightarrow \ D(5\pi/4 - \alpha) \, , \tag{3.9}
$$

which is exactly what we shall find in section 6.1.

4 Perturbative analysis

The renormalisation group equations for perturbations of conformal boundary conditions (and hence also of defects) have been known for a long time, studied first in [1] and used in [20, 28] to study the flows in unitary minimal models.

The necessary ingredients are a conformal boundary condition, a set of relevant boundary fields $S = \{\phi_i\}$ which is closed in the sense that all the relevant fields occurring in the fusion of any two fields in S is also in S, the conformal dimensions h_i of these fields, and the structure constants c_{ijk} between these relevant fields. Furthermore, since the perturbative integrals are divergent for $h_i \geq 1/2$, it is necessary to regularise them to which end we introduce a UV cut-off a as in [1] and define dimensionless couplings $\mu_i = \lambda_i a^{y_i}$ where $y_i = 1 - h_i$.

Using the regularisation in [1], the RG equations for the couplings μ_i are

$$\dot{\mu}_i = y_i \mu_i - \sum_{j,k} c_{ijk} \mu_j \mu_k + O(\mu^3) \ . \tag{4.1}$$

The change in the g-value of the boundary condition/defect is also known in perturbation theory [1, 28] and is (to third order)

$$\log(g(\mu_i)) - \log(g_0) = -\pi^2 y_i \mu_i^2 + \frac{2\pi^2}{3} \sum_{j,k} c_{ijk} \mu_i \mu_j \mu_k \ . \tag{4.2}$$

The scale dimensions of the perturbing fields at a fixed point can be read off by linearising the RG equations about the new fixed point, the eigenvalues being $1 - h'$ where h' is the scale dimension of the field [20].

We now restrict attention to the perturbed defects (2.23). In this case the space of relevant defect fields generated by ϕ and $\bar{\phi}$ closes on those fields alone, that is they generate no new relevant defect fields, so we do not need to introduce couplings to any other fields into the RG equations.

Secondly, since ϕ and $\bar{\phi}$ are chiral and anti-chiral respectively, the only structure constants appearing in the RG equations which can be non-zero[3] are $c_{\phi\phi\phi}$ and $c_{\bar{\phi}\bar{\phi}\bar{\phi}}$, and these are in fact equal and the same as the boundary structure constant $c_{\psi\psi\psi}$ for the field $\psi \equiv \psi_{(1,3)}$ on the $(1, 2)$ conformal boundary condition (see footnote 2 and [29, sect. 2]). This means that the defect RG equations are two decoupled copies of the boundary RG equations of [28], that is

$$\dot{\mu}_l = y \mu_l - c_{\psi\psi\psi} \mu_l^2 \ , \tag{4.3}$$
$$\dot{\mu}_r = y \mu_r - c_{\psi\psi\psi} \mu_r^2 \ ,$$

where $y = 1 - h_{1,3} = \frac{2}{p+1}$ and $c_{\psi\psi\psi} = \sqrt{8/3} + O(y)$. The g value of the perturbed defect is given to third order by

$$\log(g(\mu_l, \mu_r)) - \log(g(0,0)) = -\pi^2 y(\mu_l^2 + \mu_r^2) + \frac{2\pi^2}{3} c_{\psi\psi\psi} (\mu_l^3 + \mu_r^3) \ . \tag{4.4}$$

Each RG equation has two fixed points, $\mu = 0$ and $\mu = \mu^*$ (where $\mu^* = y/c_{\psi\psi\psi}$) so that the combined RG equations have four fixed points.

---

[3]It is important to note that $c_{\psi\psi\psi} \neq 0$ for $p > 3$ but when $p = 3$ the constant $c_{\psi\psi\psi}$ vanishes, so that this case is not directly amenable to the analysis here.
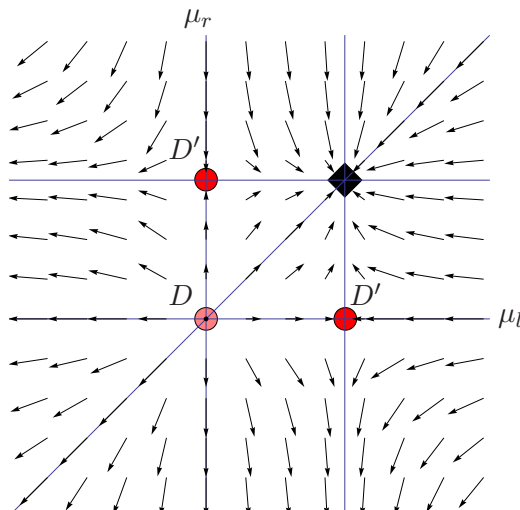
Figure 5. The perturbative flows for the system (4.3). The perturbative fixed points are as in figure 1, the black diamond being the conformal defect C.

It is important to note that the perturbation expansion is for small y, that is for large p where the central charge is close to 1. While the perturbative results for boundary flows in [28] still hold true all the way down to $p = 3$, this will not be the case here, as the spectrum of the IR fixed points is quite different at $p = 3$.

The perturbative RG flows are shown in figure 5.

The values of the couplings at the fixed points, the corresponding value of g and the scale dimensions of the perturbing fields at the fixed point (to first order in y) are given below

$$
\begin{array}{c|cccc}
(\mu_l, \mu_r) & \log(g/g_0) & h_\phi & h_{\bar{\phi}} \\
\hline
(0,0) & 0 & 1-y & 1-y \\
(\mu^*, 0) & -\frac{\pi^2 y^3}{8} & 1+y & 1-y \\
(0, \mu^*) & -\frac{\pi^2 y^3}{8} & 1-y & 1+y \\
(\mu^*, \mu^*) & -\frac{\pi^2 y^3}{4} & 1+y & 1+y
\end{array}
\tag{4.5}
$$

The topological defects of lowest g value and their expansions in y to third order are

$$
\begin{array}{c|cc}
\text{Defect} & g & \log(g) \\
\hline
D_{(1,1)}, D_{(p-1,1)} & 1 & 0 \\
D_{(2,1)}, D_{(p-2,1)} & 2\cos\left(\frac{\pi}{p}\right) & \log(2) - \frac{\pi^2 y^2}{8} - \frac{\pi^2 y^3}{8} \\
D_{(1,2)}, D_{(1,p-1)} & 2\cos\left(\frac{\pi}{p+1}\right) & \log(2) - \frac{\pi^2 y^2}{8} \\
D_{(3,1)}, D_{(p-3,1)} & 1 + 2\cos\left(\frac{2\pi}{p}\right) & \log(3) - \frac{\pi^2 y^2}{3} - \frac{\pi^2 y^3}{3} \\
D_{(1,3)}, D_{(1,p-2)} & 1 + 2\cos\left(\frac{2\pi}{p+1}\right) & \log(3) - \frac{\pi^2 y^2}{3}
\end{array}
\tag{4.6}
$$

Comparing g-values and noting that the end point of an RG flow generated by a chiral field must be topological, we see that the chiral and anti-chiral perturbations of $D_{(1,2)}$ can a priori have either the $D_{(2,1)}$ or $D_{(p-2,1)}$ defect as their perturbative fixed point. This can

– 15 –

be decided by considering two point functions of bulk fields in the presence of the defect, which can be calculated using (2.5):

$$
\begin{array}{c|ccc}
 & D_{(1,2)} & D_{(2,1)} & D_{(p-2,1)} \\
\hline
\langle \varphi_{(12,12)} | D | \varphi_{(12,12)} \rangle & -2\cos\frac{2\pi}{p+1} & -2\cos\frac{\pi}{p} & -2(-1)^p \cos\frac{\pi}{p} \\
\langle \varphi_{(21,21)} | D | \varphi_{(21,21)} \rangle & -2\cos\frac{\pi}{p+1} & -2\cos\frac{2\pi}{p} & -2(-1)^{p+1} \cos\frac{2\pi}{p}
\end{array}
\tag{4.7}
$$

We see that the two-point functions in the presence of $D_{(2,1)}$ are perturbatively close to those in the presence of $D_{(1,2)}$, whereas in the presence of $D_{(p-2,1)}$ the two point functions of $\varphi_{(12,12)}$ and $\varphi_{(21,21)}$ are not perturbatively close for p odd and p even respectively. Thus we deduce that the perturbative fixed point for the chiral perturbations of $D_{(1,2)}$ are $D_{(2,1)}$ and not $D_{(p-2,1)}$.

Equally, we see that the C defect which is the fourth fixed point in the '++' direction is not a topological defect. The question remains whether C can be found as a superposition of factorising defects or the Identity defect superposed with a set of factorising defects.

This is easy to address given the general form of a fixed point in (3.5). We first compute the g-value of each summand in (3.6)

$$
\begin{aligned}
g(D_{(a,1)} F^{s|s'}) &= \left(\frac{\sin(\frac{a\pi}{p})}{\sin(\frac{\pi}{p})} \right) \left(\frac{\sin(\frac{s\pi}{p+1})}{\sin(\frac{\pi}{p+1})} \right) \left(\frac{\sin(\frac{s'\pi}{p+1})}{\sin(\frac{\pi}{p+1})} \right) \cdot \left(\sqrt{\frac{2p}{p+1}} \frac{\sin(\frac{\pi}{p+1})}{\sin(\frac{\pi}{p})} \right) \cdot \delta \\
&= ass' \left(\sqrt{2} - \frac{3}{2\sqrt{2}} y \right) + O(y^2) .
\end{aligned}
\tag{4.8}
$$

Here δ is either $\frac{1}{2}$ or 1 as in (3.4); it does not appear in the second line as this is evaluated for fixed s, s' and large p.

Since each of the combinations $D_{(a,1)} F^{s|s'}$ has a g-value greater than or equal to one as does each of the topological defects, and since the g-value of $D_{(1,2)}$ is less than two, it is clear that any IR fixed point of a flow starting from $D_{(1,2)}$ can include at most one topological defect or one factorising combination but not both. Furthermore, for large p, the only possible factorising combinations with small enough g value are $F^{1|1}$ and $D_{(p-1,1)} F^{1|1}$ but these do not agree with the perturbative calculation of the g-value of C.

(We note here that there is an additional candidate in the case $p = 4$: the factorising defect $D_{(2,1)} F^{1|1}$ also has a g-value lower than that of $D_{(1,2)}$).

Summarising, from an analysis of g-values, C is not a linear superposition of topological defects and factorising defects and so contains a new conformal defect; the most likely result is that C is a new elementary conformal defect, but that cannot be determined from the calculations of the g value alone.

There remains the question of identifying the nature of the fields ϕ and $\bar\phi$ at the fixed points. We can do this by checking which fields on $D_{(2,1)}$ have weights as given in (4.5).

This is straightforward and the only candidates are as given below

$$
\begin{array}{c|ccc}
(\mu_l,\mu_r) & D & \phi & \bar{\phi} \\
\hline
(0,0) & D_{(1,2)} & \phi_{(13)(11)} & \phi_{(11)(13)} \\
(\mu^*,0) & D_{(2,1)} & \phi_{(31)(11)} & \phi_{(33)(13)} \\
(0,\mu^*) & D_{(2,1)} & \phi_{(13)(33)} & \phi_{(11)(31)} \\
(\mu^*,\mu^*) & C & ? & ?
\end{array}
\tag{4.9}
$$

This means that we should be able to obtain the 'C' defect by TCSA calculations starting both from $D_{(1,2)}$ and perturbing by $\phi + \bar{\phi}$ and also starting from $D_{(2,1)}$ and perturbing by $\phi_{(13,33)}$ (or equivalently by $\phi_{(33,13)}$). This is one of the subjects of section 6.

5 Truncated conformal space approach for defects

5.1 The TCSA Hamiltonian for defects

The so-called truncated conformal space approach or TCSA is a numerical method for calculating the spectrum of a perturbed conformal field theory. One chooses a system which admits a Hamiltonian description and then the Hamiltonian is restricted to a finite dimensional subspace of the infinite dimensional Hilbert space spanned by energy eigenstates whose energy eigenvalues (or conformal weights) are not greater than a threshold value. The original idea was proposed in [31] and it was applied for the first time for boundary problems in [9].

One can envisage several possible systems involving defects which allow such a Hamiltonian description. We choose to apply a generalisation of the boundary TCSA of [9], because the space of states is much smaller than in the other possibilities (they form irreducible representations of a single copy of the Virasoro algebra — see (2.10)). This makes the numerical calculations easier and we can also make use of the known properties of the interactions between defects and boundaries. The simplest situation is given by a strip of width R with conformal boundary condition $(1,1)$ on both sides and a defect labelled by $k \in \mathcal{I}_p$ running parallel to the boundaries at a distance a from one boundary. According to (2.10) the Hilbert space consists of a sole representation (independently of a),

$$
\mathcal{H}_k^{(1,1),(1,1)} = R_k \ .
\tag{5.1}
$$

By the exponential map the strip unfolds onto the upper half plane with the boundaries lying along the negative and the positive real axis and the defect line running from the origin to infinity at an angle $\theta = a\pi/R$, as shown in figure 6.

The Hamiltonian of this conformal field theory perturbed by N defect fields is

$$
H = \frac{\pi}{R}\left[L_0 - \frac{c}{24} + \sum_{i=1}^{N} \lambda_i \left(\frac{R}{\pi}\right)^{1-(h_l^i+h_r^i)} e^{i(h_l^i-h_r^i)\theta} \phi_{h_l^i,h_r^i}(e^{i\theta}, e^{-i\theta}) \right] \ .
\tag{5.2}
$$

We use a non-orthonormal basis consisting of vectors of the form

$$
L_{-n_1}\ldots L_{-n_m}|h_k\rangle \ , \qquad n_1 \geq \cdots \geq n_m > 0 \ .
\tag{5.3}
$$
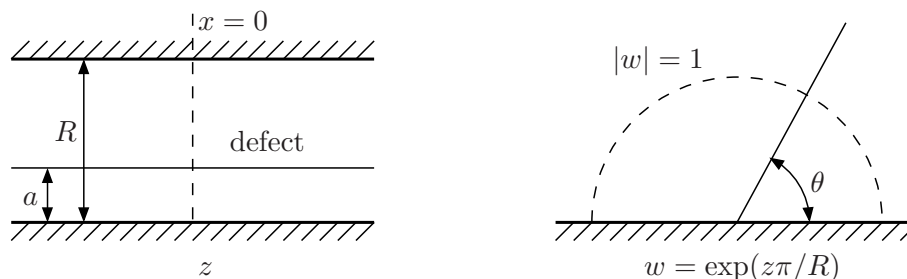
Figure 6. The strip is mapped to the upper half-plane and a defect running parallel to the edges of the strip is mapped into a defect running in a radial straight line. The dotted line shows an equal time slice for the Hamiltonian description.

We label these basis vectors $|v_i\rangle$, their L_0 eigenvalues by Δ_i and their inner product matrix $G_{ij} = \langle v_i | v_j \rangle$. The inner product matrix appears explicitly in the matrix to be diagonalised:

$$h_{jk} = \frac{\pi}{r} \left[\left(\Delta_j - \frac{c}{24} \right) \delta_{jk} + \sum_{i=1}^{N} \kappa_i \, e^{i(h_l^i - h_r^i)\theta} \, (G^{-1} B(\theta)^i)_{jk} \right], \qquad (5.4)$$

where we have introduced an energy scale Λ so that the operator $h = H/\Lambda$ is dimensionless and its matrix elements are h_{ij} where $h|v_j\rangle = h_{ij}|v_i\rangle$; furthermore, $B(\theta)_{jk}^i$ are the matrix elements $\langle v_j | \phi_{h_l^i, h_r^i}(e^{i\theta}, e^{-i\theta}) | v_k \rangle$ in the basis (5.3), $r = \Lambda R$ is a dimensionless parameter and $\kappa_i = \lambda_i (R/\pi)^{1 - h_l^i - h_r^i}$ are dimensionless coupling constants.

In the general case it is necessary to determine the structure constants to normalise the matrix elements $B(\theta)^i$ correctly, but in the cases we consider the Hilbert space consists of a single representation so that there is a single highest weight $|h_k\rangle$ and so we normalise the fields so that $\langle h_k | \phi_{h_i, \bar{h}_j}(1) | h_k \rangle = 1$.

The two special cases we will consider are the case $N = 1$ of a single non-chiral perturbation and the case $N = 2$ where the perturbing fields are two chiral perturbations (2.22) with $(h_l^1, h_r^1) = (h, 0)$ and $(h_l^2, h_r^2) = (0, h)$. In the first case, there is a single dimensionless coupling constant κ and the Hamiltonian becomes

$$\frac{r}{\pi} h_{jk} = \left(\Delta_j - \frac{c}{24} \right) \delta_{jk} + \kappa \, e^{i(h_l - h_r)\theta} \, (G^{-1} B(\theta))_{jk}. \qquad (5.5)$$

In the second case, the two coupling constants are $\kappa_l = \kappa_1 = \kappa \cos(\alpha)$ and $\kappa_r = \kappa_2 = \kappa \sin(\alpha)$ so that

$$\frac{r}{\pi} h_{jk} = \left(\Delta_j - \frac{c}{24} \right) \delta_{jk} + \kappa \left(\cos(\alpha) \, e^{ih\theta} (G^{-1} B(\theta))_{jk} + \sin(\alpha) \, e^{-ih\theta} (G^{-1} B(\theta)^*)_{jk} \right), \qquad (5.6)$$

where $B(\theta)^*$ is the complex conjugate of the matrix $B(\theta)$.

From the equality

$$(\Delta_i - \Delta_j)\langle v_i | \phi_h(z) | v_j \rangle = \langle v_i | [L_0, \phi_h(z)] | v_j \rangle = \left(h + z \frac{\partial}{\partial z} \right) \langle v_i | \phi(z) | v_j \rangle, \qquad (5.7)$$

it follows that the matrix elements of a chiral field between L_0 eigenstates have coordinate dependence

$$\langle v_i | \phi_h(z) | v_j \rangle = C \cdot z^{\Delta_i - h - \Delta_j}. \qquad (5.8)$$

This implies that

$$e^{ih\theta}B(\theta)_{kl} + e^{-ih\theta}B(\theta)^*_{kl} \propto e^{i(\Delta_k - \Delta_l)\theta} + e^{i(\Delta_l - \Delta_k)\theta} \,. \qquad (5.9)$$

When the defect is in the middle of the strip, $\theta = \pi/2$, and the couplings to the left and right fields are the same $(\cos(\alpha) = \sin(\alpha))$ then the (k, l) matrix element of the perturbing Hamiltonian is proportional to $i^{\Delta_k - \Delta_l} + (-i)^{\Delta_l - \Delta_k}$. If $\Delta_l - \Delta_k$ is an odd integer, the two terms cancel each other and the matrix element becomes exactly zero. In all our examples, the Hilbert space consists of a single representation, so the weight differences are always integers and they are odd if one of the vectors belongs to an even level while the other one belongs to an odd level. This means that for $\theta = \pi/2$ and $\kappa_l = \kappa_r$, the even and odd levels of the representation constitute two disconnected sectors: the Hamiltonian has zero matrix elements between vectors belonging to different sectors and thus it is block diagonal.

5.2 Finite-size scaling in TCSA

There are two RG-type flows at play in the TCSA system. The first is the physical flow in which we are interested, that is the flow induced by scaling the size of the system. We parametrise this flow by a parameter t. The second is that induced by changing the cutoff N limiting the size of the space of states. We are interested in the case of two relevant fields with a Hamiltonian (5.6) in which case there are three couplings to consider, $r(N, t)$ and $\kappa_i(N, t)$.

Considering the case of infinite cut-off first, we expect that the TCSA system approaches the system with canonical scaling, so that at $N = \infty$

$$\left\{ \begin{array}{l} \dot{r} = r \\ \dot{\kappa_i} = y\kappa_i \end{array} \right. \quad \text{or} \quad \left\{ \begin{array}{l} r = r_0 e^t \\ \kappa_i = \kappa_i^0 \, e^{yt} \end{array} \right. \qquad (5.10)$$

For finite N, these are both altered. This has two effects: firstly, the eigenvalues of h_{jk} are related to those of the renormalised Hamiltonian up to an unknown factor, so that it is only ratios of energy differences that can be calculated accurately; secondly, the TCSA flow can approximate IR fixed points for finite values of the bare coupling constants or equivalently a finite value of the bare volume [10], so that we can find one, or indeed more, conformal field points for increasing values of κ.

We can find the change in the coupling constants as N changes, which from [10] is according to an RG-type equation of the form

$$- N\frac{\partial \kappa_i}{\partial N}(N, t) = \tilde{\beta}_i(\kappa(N, t); N) \,, \qquad (5.11)$$

where

$$\tilde{\beta}_i(\kappa; N) = -c_{ijk}\kappa_j\kappa_k N^{-y} \, + \, o(\kappa^2, N^{-y}, y) \,. \qquad (5.12)$$

We can use this equation to find the finite-size scaling flow at fixed cut-off under two assumptions.

The first assumption, already stated, is that in the $N \to \infty$ limit, the TCSA couplings become the "linear beta function" couplings, a fact assumed in much of the literature, so that the finite-size flow at $N = \infty$ is

$$\kappa_i(\infty, t) = e^{yt}\, \kappa_i^0 \; . \tag{5.13}$$

The second assumption is that the leading terms in the beta-functions take a simple scaling form, that is

$$\tilde{\beta}_i(\kappa; N) = N^y \gamma_i(\kappa N^{-y}) + \dots \; . \tag{5.14}$$

This is true for the quadratic terms and a reasonable assumption for the leading behaviour of the higher order terms.

Given these two assumptions, we can then deduce the following three results (see appendix B)

$$\kappa_i(Ne^t, t) = e^{yt}\, f_i(\kappa^0) \tag{5.15}$$

$$\kappa_i(N, t) = e^{yt}\, \kappa_i(Ne^{-t}, 0) \tag{5.16}$$

$$\frac{\partial}{\partial t}\kappa_i(N, t) = \beta_i(\kappa(N, t); N) \tag{5.17}$$

The first result states that we can follow a finite-size scaling flow by scaling the couplings by the same factor but also increasing the cut-off. This is useful if we do not know the beta-functions, as is the case here. The second result gives the scaling flow at fixed N in terms of the couplings at smaller N, and the third result states that the finite-size flow at a fixed cut-off is governed by a standard beta-function relation, where the functions are simply related to those for the change in N:

$$\beta_i(\kappa; N) = y\kappa_i + \tilde{\beta}_i(\kappa; N) \; . \tag{5.18}$$

Finally, a conformal defect corresponds to a zero of the beta-functions $\beta_i(\kappa; N)$. From the leading behaviour (5.14), the positions of the zeroes $\kappa^* a(N)$ scale approximately with N as N^y which we check in one case in section 6.

Given the TCSA Hamiltonian, it is possible to calculate the TCSA approximation of many different physical quantities, but in this paper we have examined only one, namely the spectrum of the Hamiltonian, and we describe in the next section how we use this to identify the presence of possible RG fixed points, that is conformal defects, and attempt to identify them.

5.3 Identification of conformal defects using TCSA

From the TCSA method, we obtain the spectrum of the Hamiltonian on a strip. The simplest way to identify candidate conformal defects is to place the defect in the middle of the strip and use the fact that in this case the partition function takes the special form (2.16) and the spectrum is organised into representations of the Virasoro algebra of central charge $2c$. Consequently, we examine the TCSA results to find spectra which take this special form and propose these as candidates for conformal defects.

To be explicit, we consider the model on a strip of width R with conformal boundary conditions on the two edges and the defect D in the middle. In our TCSA calculations we will always take the boundary condition to be the same on both edges, but for the moment we shall label them B and B' for generality. This system can be folded into the folded model of central charge $2c$ on a strip of width $R/2$ with a factorised boundary condition (B, B') on one edge and a boundary condition corresponding to the defect on the other edge. If this defect is conformal, then the spectrum falls into representations of the Virasoro algebra of charge $2c$ and

$$Z_{(B,B');D_{\text{conformal}}} = \sum_h m_h \chi_{h,2c}(q) , \qquad (5.19)$$

where $q = \exp(-2\pi L/R)$. This means that the spectrum falls into sets of levels separated by integer multiples of $2\pi/R$ with distinctive multiplicities. If these are absent, then the defect D cannot be conformal.

For the two special cases of a topological defect and a factorised defect the spectrum takes more particular forms.

If the defect D is a topological defect then the partition function is simply that of the original model on a strip of width R with two conformal boundary conditions, so that

$$Z_{(B,B');D_{\text{topological}}} = \sum_i m_i \chi_{i,c}(\sqrt{q}) . \qquad (5.20)$$

In this case, the spectrum falls into sets of levels separated by integer multiples of π/R, which is half the spacing of the energy levels in the general case.

If the defect D is in fact a factorised defect of the form (2.12) then the partition function takes the special form

$$Z_{(B,B');D_{\text{factorised}}} = \sum_{a,b,i,j} \left(n_{ab} N_{Ba}^i N_{B'b}^j \right) \chi_{i,c}(q) \chi_{j,c}(q) . \qquad (5.21)$$

In this case, the spectrum falls into sets of levels separated by integer multiples of $2\pi/R$ as in the general case but with typically much higher degeneracies than those of a general conformal defect.

A further check can be obtained by moving the defect across the strip to different angles θ. For topological defects the spectrum should be independent of θ while for purely factorising defects $F = \sum_{a,b} n_{ab} \| a \rangle\!\rangle \,\langle\!\langle b \|$ the partition function is

$$Z_{(B,B');D_{\text{factorised}}}(q;\eta) = \sum_{a,b,i,j} \left(n_{ab} N_{Ba}^i N_{B'b}^j \right) \chi_{i,c}\left(q^{\frac{1}{2\eta}} \right) \chi_{j,c}\left(q^{\frac{1}{2(1-\eta)}} \right), \quad \theta = \eta\,\pi , \quad (5.22)$$

which lets us identify the coefficients n_{ab} exactly.

6   TCSA results

We consider two different systems: firstly the Ising model, as a check on our method and confirming the results of [11]; secondly, we consider minimal models with p large for which we take $p = 10$ as a typical example. Throughout this section we use the dimensionless couplings κ_i as appropriate to the TCSA method.
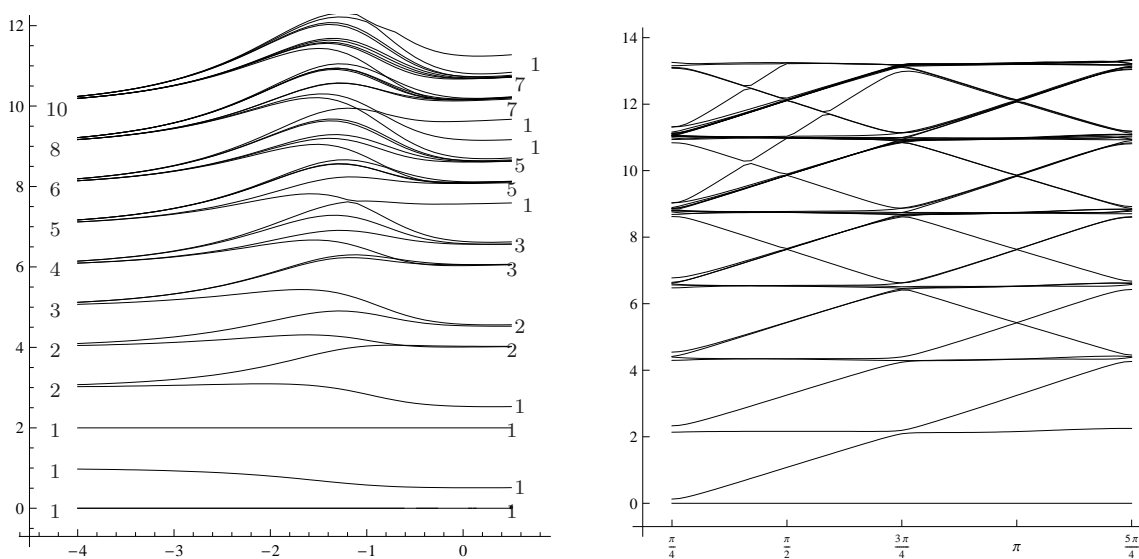
(a) TCSA results in $M(3,4)$ for $\alpha = 3\pi/8$ plotted against $\log(\kappa)$ for $N = 24$ and 762 states. The degeneracies of the energy levels at the IR fixed point are grouped according to the representation of the $c = 1$ folded model into which they fall.

(b) The spectrum of $M(3,4)$ at $\log(\kappa) = 0.3$ as a function of α for for $\pi/4 \leq \alpha \leq 5\pi/4$ with $N = 24$ and 762 states.

Figure 7. IR fixed points in the critical Ising model.

6.1 The critical Ising model

Using the defect TCSA method we can check the predictions of [11] as well as the accuracy of the TCSA method. We recall that [11] predict flows of the form $D_\sigma \to N(5\pi/4 - \alpha)$ where

$$\tan(\alpha) = \kappa_r/\kappa_l \,, \tag{6.1}$$

As an example, we calculate the TCSA spectrum for $\alpha = 3\pi/8$ and compare it with the partition function at $\varphi_0 = 5\pi/4 - 3\pi/8 = 7\pi/8$ given in (3.7)

$$Z_{D(0)_+,D(7\pi/8)}\left(q; \frac{1}{2}\right) = q^{\frac{49}{128}-\frac{1}{24}}\left(1 + q^{\frac{1}{4}} + q + q^{\frac{5}{4}} + 2q^2 + 2q^{\frac{9}{4}} + 3q^3 + 3q^{\frac{13}{4}} \right. \tag{6.2}$$
$$\left. + q^{\frac{15}{4}} + 5q^4 + 5q^{\frac{17}{4}} + q^{\frac{9}{2}} + q^{\frac{19}{4}} + 7q^5 + \dots \right) \,.$$

In figure 7(a) the normalised energy differences $2(E_i - E_0)/(E_2 - E_0)$ are shown against the logarithm of the dimensionless coupling strength κ of the perturbation. With this normalisation, the indicator of an IR fixed point is the existence of a state with normalised gap 4. The only such point visible is that with $\log(\kappa) \sim 0.3$. At this point, the energy levels visible have rearranged themselves into four distinct sets and both this arrangement and the values of the energy gaps agree with the partition function (6.2). We conclude that the endpoint of the flow starting at the angle $\alpha = 3\pi/8$ in the (κ_l, κ_r) plane is indeed the conformal defect $D(5\pi/4 - 3\pi/8) = D(7\pi/8)$.

The IR fixed point is located at a finite value of the bare coupling constant and at approximately the same distance from the origin in every direction. This means we can

N	10	12	14	16	18	20	22
$\log(\kappa^*_{\text{measured}})$	-1.51	-1.46	-1.43	-1.40	-1.37	-1.35	-1.33
$\log(\kappa^*_{\text{theory}})$	-1.46	-1.43	-1.40	-1.38	-1.35	-1.34	-1.32

Table 1. The approximate position of the perturbative fixed point in $M(10,11)$ in the purely chiral direction as a function of TCSA cut-off N.

view all the IR fixed points together by plotting the energy differences $\frac{r}{\pi}(E_i - E_0)$ against the angle α at this fixed value of κ. Expanding the partition function (3.7) gives

$$Z_{D(0)_+, D(\varphi_0)}\left(q; \frac{1}{2}\right) = q^{\frac{x^2}{2} - \frac{1}{24}}\left(1 + q^{2-2x} + q + q^{3-2x} + 2q^2 + 2q^{4-2x} + q^{2+2x} + \dots\right),$$
(6.3)

where $x = \varphi_0/\pi$. This means that the energy gaps are straight lines as functions of φ_0 or α and this is exactly what can be seen in the TCSA plot (figure 7(b)). The fact that these lines are straight also implies that κ_1/κ_2 is a constant along the finite-size scaling flow. This is not expected to be the case in general, but the extra symmetry in the Ising model allows this to happen.

This result provides a very strong indication that our identification of the RG flow fixed points in terms of Dirichlet-type defects is correct, confirming both the calculations of [11] and the usefulness of the TCSA method.

6.2 Minimal models with $p > 3$

For the minimal models $M(p, p+1)$ with $p > 3$ the flow picture is different from that for the critical Ising model, as is to be expected from the RG analysis. The proposed landscape of flows can be seen in figure 1. In the following we illustrate the exploration of this picture using the $M(10, 11)$ model with TCSA.

6.2.1 Chiral perturbations

The simplest cases are the purely chiral perturbations. The spectra for these models are both formally and numerically identical to the corresponding boundary perturbations as is explained in section 2.4. From section 3.1 we see that the IR fixed points in the positive and negative directions are the $(2, 1)$ and the $(1, 1)$ defects, respectively. These defect flows are shown in figure 8 where the normalised energy differences are plotted against the logarithm of the coupling strength. In the positive direction the cut-off effects drive the flow past the first fixed point to a second one, realising the reversed version of the $(1, 3) \to (2, 1)$ flow. Since the spectra are numerically identical to those in the boundary case, this effect is identical to that observed for boundary flows in [10].

In the perturbative direction we can estimate the location of the TCSA fixed point as the value of κ for which the fourth and fifth energy levels cross and this depends on N as given in table 1. As can be seen it is very close to the approximate value predicted by the analysis in [10] which gives $\kappa^* \approx 0.1526 N^y$, once the different normalisation of the TCSA perturbing field is taken into account.

(a) Positive direction: $(1,2) \to (2,1) \leftarrow\!- (1,3)$. (b) Negative direction: $(1,2) \to (1,1)$.
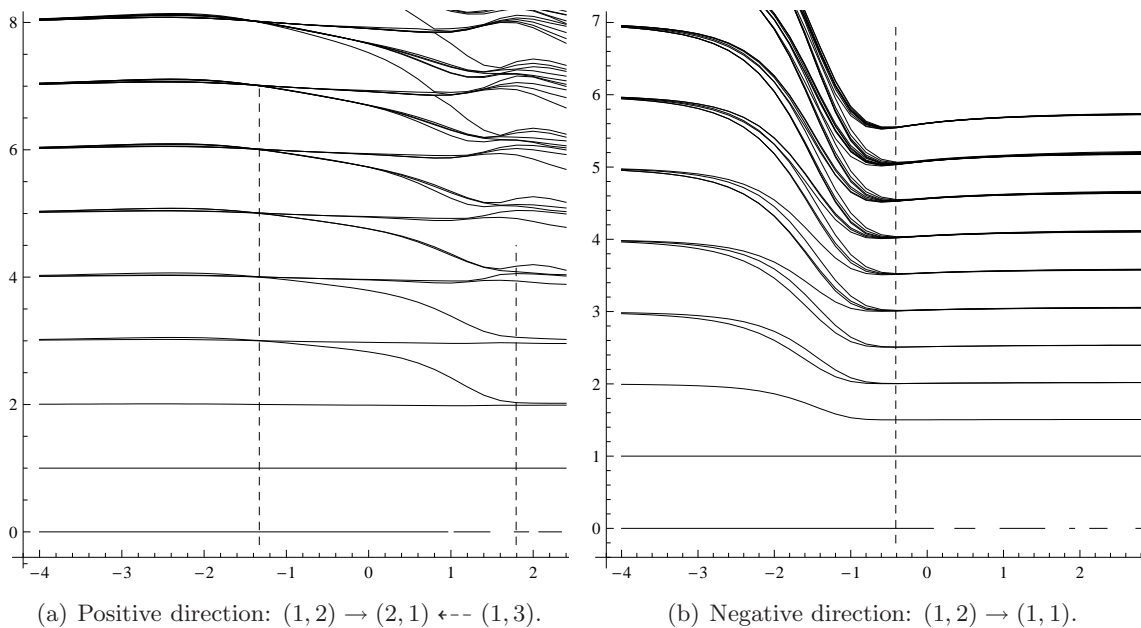
Figure 8. $M(10,11)$: chiral flows. We show the normalised energy levels plotted against $\log(\kappa)$ with $N = 22$, 1794 states.

### 6.2.2 The third quadrant: $\kappa_l < 0$, $\kappa_r < 0$

Next we turn to the third quadrant of the plane of the couplings in figure 1. We have searched thoroughly for fixed points in the domain of convergence of TCSA and found a single fixed point F, which is in the diagonal direction $\kappa_l = \kappa_r < 0$.

As discussed in section 5.1, the TCSA Hamiltonian for $\kappa_l = \kappa_r$ is block diagonal and the flows for the two sectors are shown in figure 9. We find that for large κ the spectrum approaches an IR fixed point for which the eigenstates in each sector separately fit into representations of the folded model.

Combining the two sectors is a non-trivial task, because they have different effective cut-offs. This means that they have different values for the non-universal boundary energy and different re-scalings of the couplings κ and r so that the two sectors cannot be directly compared. The usual perturbative renormalisation based on minimal subtraction or analytic continuation cannot be implemented within the TCSA framework, but it is possible to define a prescription for the relative shift of the sectors. Going from a TCSA cut $N = 2n$ to $N = 2n + 1$ the even energy levels are not affected, because the new states in the Hilbert space belong to the odd sector. Similarly, raising the cut from $N = 2n + 1$ to $N = 2n + 2$ the odd levels do not change. One can define, say, the values of the even eigenvalues at the odd cut $N = 2n + 1$ as

$$e_i^{\text{even}}(2n + 1) = \frac{1}{2} \left(e_i^{\text{even}}(2n) + e_i^{\text{even}}(2n + 2) \right) . \tag{6.4}$$

The justification of this prescription is provided by its application to the fixed point F where it yields the spectrum shown in figure 9. It corresponds to a partition function of
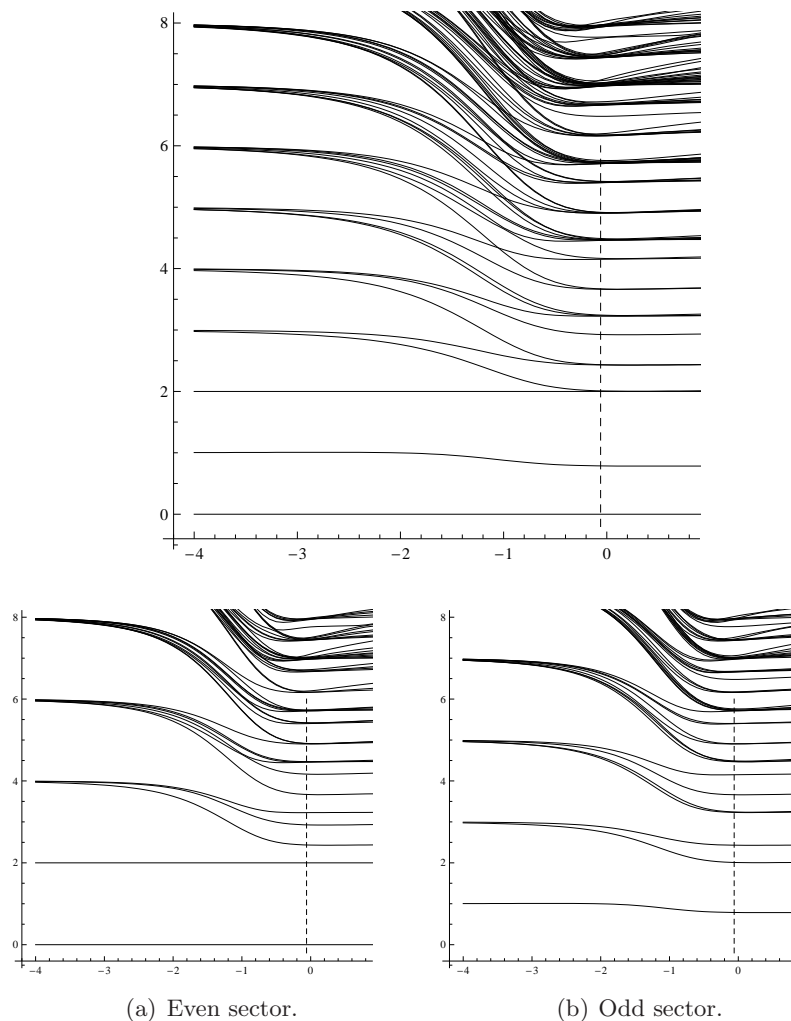
Figure 9. $M(10, 11)$: diagonal flow in the negative direction. In the main figure, the scaled energy gaps for both sectors are shown, the odd sector with TCSA cut 19 and the even sector given by the combination of cuts 18 and 20 as detailed in the text. The small sub-figures show the even and odd sectors separately.
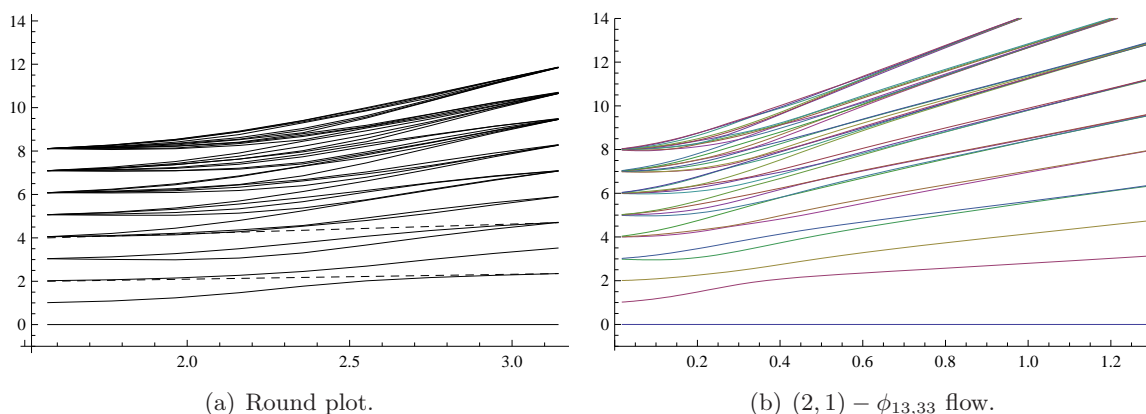
the form (5.22) with $\eta = 1/2$, namely

$$Z_F(q; \frac{1}{2}) = \sum_{r=1}^{9} \chi_{r,1}(q)^2 \,, \tag{6.5}$$

although we could not identify all the components as some of them enter only at high level.

This implies that

the IR fixed point in the negative diagonal direction is the factorising defect

$$F = \sum_{r=1}^{p-1} ||r, 1\rangle\rangle\langle\langle r, 1|| \,.$$

(a) Round plot.   (b) $(2,1) - \phi_{13,33}$ flow.

Figure 10. $M(10,11)$: comparison between the $(2,1) - \phi_{13,33}$ flow and the round plot. The absence of states of scaled energy 2 and 4 means that there is no indication of a conformal fixed point between the points $\alpha = \pi/2$ and $\alpha = \pi$. The different slopes of the lines is a result of the different renormalisations of the function $r(\kappa)$ in the two systems.

We found the same result for other minimal models and we checked also that the dependence of the spectrum on the position of the defect is as it is expected and given by (5.22). Note that the defect F is of the form of (3.5) with $s = s' = 1$.

6.2.3 The second and fourth quadrants: κ_l and κ_r of opposite signs

For different signs of the couplings κ_l and κ_r we found strong indications of a fixed point far from the perturbative region which appears to be a deformation of the (ff) fixed point in the Ising model; we call this conformal defect $(ff)'$. However, since this is far from the perturbative region, there is no necessity that this be reachable by a finite-size scaling flow from the defect D, and indeed we believe that all RG flows starting at D in this quadrant end up at the identity defect I. This is the result predicted by the simple model in section 7 and to test it we explored the quadrant by making "round plots" similar to the Ising model, that is plots of the spectrum as functions of α at various fixed κ for the Hamiltonian (5.6). In figure 10(a) the weight differences are plotted against the angle α, defined in the same way as for the Ising model in (6.1), with $\log(\kappa)$ interpolating between the approximate fixed point values $\log(\kappa^*) = -1.4$ at $\theta = \pi/2$ and $\log(\kappa^*) = -0.4$ at $\theta = \pi$. The plot does not feature any fixed points but looks like a flow interpolating the chiral fixed points $(2,1) \rightarrow (1,1)$ located on the vertical and horizontal axes. This picture can be compared with an actual flow starting from the defect $(2,1)$. As can be seen in (4.9), in first order perturbation theory the field ϕ transforms into the relevant field $\phi_{(13)(33)}$ along the flow $(1,2) \rightarrow (2,1)$ triggered by $\bar{\phi}$. It is possible to study the flow starting from the defect $(2,1)$ generated by the non-chiral perturbation $\phi_{(13)(33)}$ in TCSA; some details of the method are given in appendix C. For negative values of the perturbation the flow is shown in figure 10(b). It looks very much the same as the round plot, as shown in the schematic figure 12(a).

This tells us that:

All RG flows starting from the defect D with κ_l and κ_r of opposite signs end at the identity defect I, and the boundary of this space of flows is an RG flow from $D_{(2,1)}$ to I.
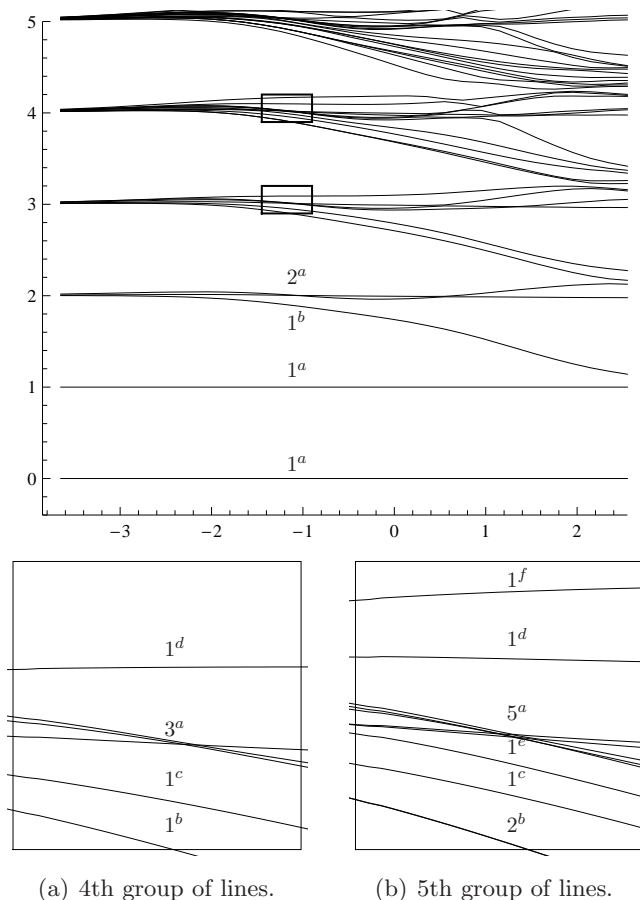
Figure 11. $M(10, 11)$: diagonal flow in the positive direction, even sector, scaled energy gaps vs $\log(\kappa)$ for a strip of width π truncated at level 20; the boxed regions are shown enlarged in the two smaller figures. The energy levels at the fixed point can grouped into representations of the folded model and are labelled m^l where m is the degeneracy and l is the label of the representation.

6.2.4 The first quadrant $\kappa_l > 0$, $\kappa_r > 0$

Based on perturbation theory we expect a non-topological fixed point C in the diagonal direction $\kappa_l = \kappa_r > 0$. We can apply the tools used in the previous cases for exploring the flows in the first quadrant. In figure 11 the normalised energy differences are plotted against the logarithm of the coupling strength in the positive diagonal direction for the even sector. We find multiple degeneracies at $\log(\kappa) \sim -1.2$ indicating the presence of a conformal fixed point. One feature of this fixed point characteristic of a perturbative fixed point is that the energy levels stay close to their UV values, so that lines appear to split apart initially then to rejoin and intersect with multiple degeneracies at κ^*.

As shown in the magnified plots of the regions around the fixed point, the states approximately group into representations of the folded model with the correct multiplicities. An analogous pattern of line crossings is also seen in the odd sector.
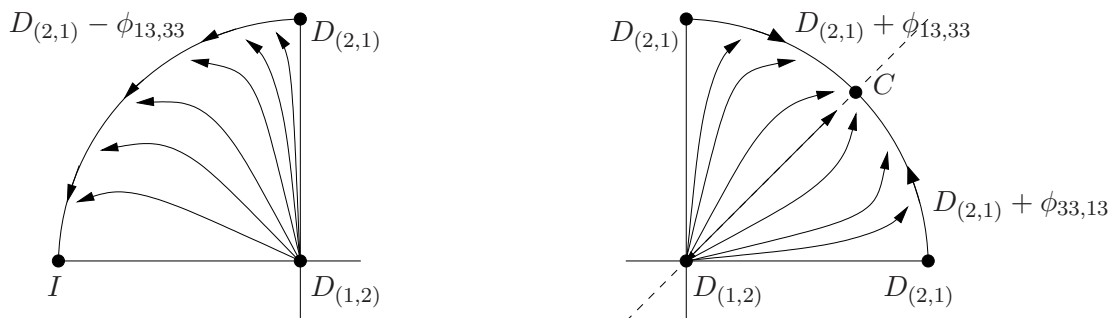
(a) The conjectured exact flow from $D_{(2,1)}$ to $I = D_{(1,1)}$ and the set of flows starting from $D_{(1,2)}$ for various values of α in the second quadrant.

(b) The conjectured exact flow from $D_{(2,1)}$ to C and the set of flows starting from $D_{(1,2)}$ for various values of α in the first quadrant.

Figure 12. The conjectured flows in the first and second quadrants.

From the perturbative picture we also expect all flows starting with $\kappa_l > 0, \kappa_r > 0$ to flow to C and the boundary of this space of flows to be be a pair of flows starting from the two $D_{(2,1)}$ defects generated by $\phi_{(13;33)}$ for $\alpha > \pi/4$ and by $\phi_{(33;13)}$ for $\alpha < \pi/4$. We have again checked this by comparing "roundplots" in the two-parameter space at fixed κ and varying α with the one-parameter TCSA flows $D_{(2,1)} + \phi_{(13,33)}$ and $D_{(2,1)} + \phi_{(33,13)}$, finding again qualitative agreement and support for the picture shown in figure 12(b).

As the level p of the model $M(p, p+1)$ is reduced, the TCSA results become less convincing as the new conformal fixed point moves further away from the UV fixed point. The last model for which there is convincing evidence of the new defect C is $M(5, 6)$; in model $M(4, 5)$ the triple line intersection seen in figure 11(a) is no longer seen in TCSA at the truncation levels we have been able to achieve. It is possible that increasing the truncation level would show signs of a conformal fixed point, or the position of the conformal fixed point may have moved a large distance; at the moment we cannot tell.

7 Conclusion

For $p \gg 3$, the perturbative analysis carried out in section 4 and the numerical work in section 6 suggests the pattern of flows shown in figure 13(b). We conclude that for $p \gg 3$ there is at least one IR fixed point which is a conformal defect that is neither topological nor just a sum over conformal boundary conditions, namely the one in the $\kappa_r = \kappa_l > 0$ direction.

The Ising model $M(3, 4)$ behaves differently form the other minimal models and is treated separately in section 6.1, with the pattern of flows 13(a). For $p = 3$, the fixed points that have been identified for large p all still remain, but are now just particular points in a continuum.

For p small but greater than 3, the situation is not so clear-cut. We are still not sure exactly how the fixed-points approach the $c = 1/2$ continuum, which in part is due to the numerical inaccuracies of the TCSA method.
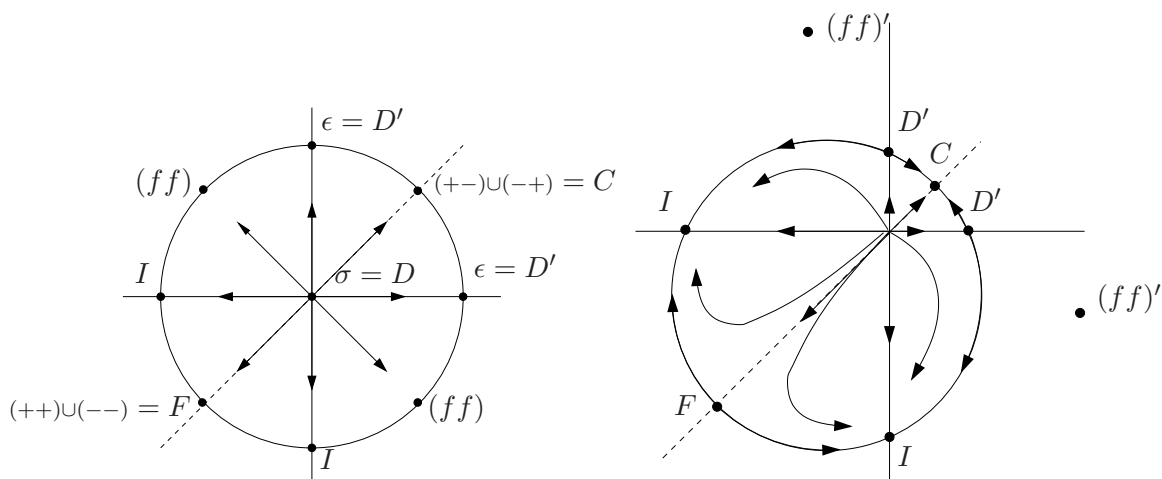
(a) The finite-size scaling flows in the Ising model showing the ring of conformal defects as a function of α with the identification of the factorised and topological defects.

(b) The conjectured pattern of flows out of the defect $D_{(1,2)}$ showing the 6 IR fixed points for $M(p, p+1)$ with p large.

Figure 13. Finite-size scaling flows.

The one-loop beta functions as discussed in section 4 predict the perturbative fixed points that we find with the TCSA analysis. It is tempting to try to extend this analysis to higher loop order to see if they confirm the RG flow structure we suggest in this paper. As a starting point, we consider the Ising model and then the changes that are present in the higher minimal models. Given the symmetries of the Ising model, the absence of three-point couplings and the continuum of fixed points, the RG flows away from the D defect can be modelled by the beta functions

$$\begin{pmatrix} \dot{\kappa_l} \\ \dot{\kappa_r} \end{pmatrix} = \frac{1}{2} \begin{pmatrix} \kappa_l \\ \kappa_r \end{pmatrix} - d(\kappa_l^2 + \kappa_r^2) \begin{pmatrix} \kappa_l \\ \kappa_r \end{pmatrix} , \tag{7.1}$$

where d is a scheme-dependent constant. This has the required $O(2)$ symmetry and a ring of fixed points at $\kappa_l^2 + \kappa_r^2 = 1/(2d)$. The minimal models $M_{p,p+1}$ with $p > 3$ have non-zero three point couplings and so the simplest change to these beta functions to incorporate these is

$$\begin{pmatrix} \dot{\kappa_l} \\ \dot{\kappa_r} \end{pmatrix} = y \begin{pmatrix} \kappa_l \\ \kappa_r \end{pmatrix} - c \begin{pmatrix} \kappa_l^2 \\ \kappa_r^2 \end{pmatrix} - d(\kappa_l^2 + \kappa_r^2) \begin{pmatrix} \kappa_l \\ \kappa_r \end{pmatrix} . \tag{7.2}$$

This breaks the degeneracy and (for $dy > 0$) has six non-trivial fixed points with the same pattern of flows that we have found, which is additional evidence in favour of the pattern we propose.

There are also various physical quantities which we would like to calculate using the TCSA method which for various reasons have proved intractable, such as the expectation values of T and $\bar{T}$ (which would give a better test of a conformal defect than the examination of the spectrum) or the reflection and tranmission coefficients defined in [26].

Finally, it appears likely that a qualitative description of the space of defects and defect flows can be found from the microscopic RSOS model description of the minimal models, something we plan to address in the future.

Acknowledgments

A Defect operators commuting with $D_{(r,1)}$

Let $\delta(s, s')$ be $1/2$ if $s = s' = \frac{p+1}{2}$ and 1 otherwise, as in the definition of $F^{s|s'}$ in (3.4). To see that $F^{s|s'}$ commutes with the topological defects $D_{(r,1)}$ one simply computes

$$
\begin{aligned}
D_{(r,1)} F^{s|s'} &= \sum_{t,u=1}^{p-1} N_{(r,1)(t,1)}^{(u,1)} D_{(u,1)} \| 1, s \rangle\!\rangle \langle\!\langle 1, s' \| D_{(t,1)} \cdot \delta(s, s') \\
&= \sum_{u=1}^{p-1} D_{(u,1)} \| 1, s \rangle\!\rangle \langle\!\langle 1, s' \| D_{(u,1)} D_{(r,1)} \cdot \delta(s, s') = F^{s|s'} D_{(r,1)} \ .
\end{aligned}
\tag{A.1}
$$

To establish the decomposition (3.5) of a conformal defect that commutes with $D_{(2,1)}$ (and hence with all $D_{(r,1)}$) it is enough to show that we can find constants $m_a^{s|s'}$ in (3.6) such that

$$
\big(C, \| a \rangle\!\rangle \langle\!\langle b \| \big) = \big(F, \| a \rangle\!\rangle \langle\!\langle b \| \big) \quad \text{for all } a, b \in \mathcal{I}_p \ .
\tag{A.2}
$$

Because of the identity $\| r, s \rangle\!\rangle = \| p - r, p + 1 - s \rangle\!\rangle$ it suffices to verify this for factorising defects of the form $\| x, v \rangle\!\rangle \langle\!\langle y, v' \|$ with $v \leq \frac{p+1}{2}$ and $v' \leq \frac{p+1}{2}$.

For the left hand side of (A.2) we find

$$
\begin{aligned}
\big(C, \| x, v \rangle\!\rangle \langle\!\langle y, v' \| \big) &= \big(C D_{(y,1)}, \| x, v \rangle\!\rangle \langle\!\langle 1, v' \| \big) = \big(C, D_{(y,1)} \| x, v \rangle\!\rangle \langle\!\langle 1, v' \| \big) \\
&= \sum_{a=1}^{p-1} N_{(y,1)(x,1)}^{(a,1)} \big(C, \| a, v \rangle\!\rangle \langle\!\langle 1, v' \| \big) \ .
\end{aligned}
\tag{A.3}
$$

To reproduce this result with $\big(F, \| x, v \rangle\!\rangle \langle\!\langle y, v' \| \big)$ we will distinguish four cases, namely whether v and v' are less or equal to $\frac{p+1}{2}$, respectively. Of course, the three cases where either v or v' are equal to $\frac{p+1}{2}$ can occur only for p odd. We will abbreviate

$$
q = \frac{p+1}{2} \ .
\tag{A.4}
$$

For $m_a^{s|s'}$ we make the ansatz

$$m_a^{s|s'} = \mu(s,s') \cdot \big(C, \|a,s\rangle\!\rangle \langle\!\langle 1,s'\| \big), \tag{A.5}$$

where $\mu(s,s') = \frac{1}{2}$ if at least one of s, s' is equal to q, and $\mu(s,s') = 1$ otherwise. The $m_a^{s|s'}$ have the property that for all s, s',

$$m_a^{q|s'} = m_{p-a}^{q|s'} \quad \text{and} \quad m_a^{s|q} = m_{p-a}^{s|q} . \tag{A.6}$$

The first equality is an immediate consequence of $\|a,q\rangle\!\rangle = \|p-a,q\rangle\!\rangle$, while for the second one we need to commute the defect operators $D_{(p,1)}$ and C and use $\langle\!\langle p,q\| = \langle\!\langle 1,q\|$,

$$m_{p-a}^{s|q} = \frac{1}{2}\big(C, D_{(p,1)}\|a,s\rangle\!\rangle \langle\!\langle 1,q\| \big) = \frac{1}{2}\big(CD_{(p,1)}, \|a,s\rangle\!\rangle \langle\!\langle 1,q\| \big) \tag{A.7}$$
$$= \frac{1}{2}\big(C, \|a,s\rangle\!\rangle \langle\!\langle 1,q\| D_{(p,1)} \big) = \frac{1}{2}\big(C, \|a,s\rangle\!\rangle \langle\!\langle 1,q\| \big) = m_a^{s|q} .$$

From their definition it is easy to check that the factorising defects $F^{s|s'}$ obey the identities

$$F^{p+1-s|p+1-s'} = F^{s|s'} \quad , \quad D_{(a,1)} F^{p+1-s|s'} = D_{(p-a,1)} F^{s|s'} . \tag{A.8}$$

This allows us to restrict the range of the s and s' summation in (3.6) to $s, s' \leq q$. We will now establish the equality (A.2) in the four cases.

i) $v, v' < q$: then

$$\big(F, \|x,v\rangle\!\rangle \langle\!\langle y,v'\| \big) = \sum_{s,s'=1}^{\lfloor q \rfloor} \sum_{a,t=1}^{p-1} m_a^{s|s'} \delta(s,s') \big(D_{(a,1)}D_{(t,1)}\|1,s\rangle\!\rangle \langle\!\langle 1,s'\| D_{(t,1)}, \|x,v\rangle\!\rangle \langle\!\langle y,v'\| \big)$$
$$= \sum_{s,s'=1}^{\lfloor q \rfloor} \sum_{a,t,u=1}^{p-1} m_a^{s|s'} N_{(a,1)(t,1)}^{(u,1)} \delta(s,s') \big(\|u,s\rangle\!\rangle \langle\!\langle t,s'\|, \|x,v\rangle\!\rangle \langle\!\langle y,v'\| \big)$$
$$= \sum_{a}^{p-1} \big(C, \|a,v\rangle\!\rangle \langle\!\langle 1,v'\| \big) N_{(a,1)(y,1)}^{(x,1)} , \tag{A.9}$$

where in the last step we used that since $s, v < q$, $\|u,s\rangle\!\rangle = \|x,v\rangle\!\rangle$ if and only if $u = x$ and $s = v$, and similarly for $\langle\!\langle t,s'\|$ and $\langle\!\langle y,v'\|$. Since $v, v' < q$ this implies also $\delta(s,s') = 1$. The above expression is equal to (A.3) by the symmetries of the minimal model fusion rules.

ii) $v < q, v' = q$: then

$$\big(F, \|x,v\rangle\!\rangle \langle\!\langle y,q\| \big) = \sum_{s,s'=1}^{\lfloor q \rfloor} \sum_{a,t,u=1}^{p-1} m_a^{s|s'} N_{(a,1)(t,1)}^{(u,1)} \delta(s,s') \big(\|u,s\rangle\!\rangle \langle\!\langle t,s'\|, \|x,v\rangle\!\rangle \langle\!\langle y,q\| \big)$$
$$= \sum_{a=1}^{p-1} m_a^{v|q} \delta(v,q) \left(N_{(a,1)(y,1)}^{(x,1)} + N_{(a,1)(p-y,1)}^{(x,1)} \right)$$
$$= \sum_{a=1}^{p-1} m_a^{v|q} N_{(a,1)(y,1)}^{(x,1)} + \sum_{a=1}^{p-1} m_{p-a}^{v|q} N_{(a,1)(y,1)}^{(x,1)} , \tag{A.10}$$

where we used that $N_{(a,1)(p-y,1)}^{(x,1)} = N_{(p-a,1)(y,1)}^{(x,1)}$. Since $m_{p-a}^{v|q} = m_a^{v|q}$, the factor of $\frac{1}{2}$ in (A.5) ensures that both sums combine to give (A.3).

– 31 –

iii) $v = q, v' < q$: this case works along the same lines.

iv) $v = q, v' = q$: then

$$
\begin{aligned}
(F, \| x, q \rangle\!\rangle \langle\!\langle y, q \|) &= \sum_{s,s'=1}^{\lfloor q \rfloor} \sum_{a,t,u=1}^{p-1} m_a^{s|s'} N_{(a,1)(t,1)}^{(u,1)} \delta(s,s') \left(\| u, s \rangle\!\rangle \langle\!\langle t, s' \|, \| x, q \rangle\!\rangle \langle\!\langle y, q \| \right) \\
&= \sum_{a=1}^{p-1} m_a^{q|q} \cdot \frac{1}{2} \cdot \left(N_{(a,1)(y,1)}^{(x,1)} + N_{(a,1)(p-y,1)}^{(x,1)} + N_{(a,1)(y,1)}^{(p-x,1)} + N_{(a,1)(p-y,1)}^{(p-x,1)} \right) \\
&= \sum_{a=1}^{p-1} m_a^{q|q} \left(N_{(a,1)(y,1)}^{(x,1)} + N_{(a,1)(p-y,1)}^{(x,1)} \right)
\end{aligned}
\tag{A.11}
$$

where we used that $N_{(a,1)(p-y,1)}^{(p-x,1)} = N_{(a,1)(y,1)}^{(x,1)}$. The rest of the argument is as in ii).

B The renormalisation group and finite-size scaling relations in TCSA

In this section we derive the form of the finite-size scaling flow in TCSA given in equations (5.15)–(5.17). We start from the three assumptions in section 5.2: if $\kappa_i(N,t)$ are the TCSA coupling constants along a finite-size scaling flow parametrised by t at cut-off N, then we assume

$$
\kappa_i(\infty, t) = e^{yt} \kappa_i^0 \,,
\tag{B.1}
$$

$$
-N \frac{\partial \kappa_i}{\partial N}(N,t) = \tilde{\beta}_i(\kappa(N,t); N) \,,
\tag{B.2}
$$

$$
\tilde{\beta}_i(\kappa; N) = N^y \gamma_i(\kappa N^{-y}) \,.
\tag{B.3}
$$

Firstly we remove the expected t dependence from $\kappa_i(Ne^t, t)$ and define

$$
\sigma^i(N,t) = e^{-yt} \kappa_i(Ne^t, t) \,.
\tag{B.4}
$$

This satisfies the differential equation

$$
-N \frac{\partial}{\partial N} \sigma^i(N,t) = N^y \gamma_i(N^{-y}\sigma) \,,
\tag{B.5}
$$

with initial conditions

$$
\sigma_i(\infty, t) = \kappa_i^0 \,.
\tag{B.6}
$$

Since both the initial conditions and the differential equation are independent of t, the solution is also independent of t and we find that

$$
\sigma_i(N,t) = f_i(\kappa_j^0; N) \,.
\tag{B.7}
$$

Substituting this into (B.4) we find our first result,

$$
\kappa_i(Ne^t, t) = e^{yt} f_i(\kappa_j^0; N) = e^{yt} \kappa_i(N, 0) \,.
\tag{B.8}
$$

Rescaling N in this equation gives the second result

$$\kappa_i(N, t) = e^{yt} \kappa_i(Ne^{-t}, 0) \, . \tag{B.9}$$

Finally, differentiating this with respect to t at fixed level N_0 gives

$$
\begin{aligned}
\frac{\partial}{\partial t} \kappa_i(N_0, t) &= y e^{yt} \kappa_i(N_0 e^{-t}, 0) - e^{yt} N_0 e^{-t} \frac{\partial \kappa_i}{\partial N}(N_0 e^{-t}, 0) \\
&= y \kappa_i(N_0, t) + e^{yt} \tilde{\beta}_i(\kappa_i(N_0 e^{-t}, 0); N_0 e^{-t}) \\
&= y \kappa_i(N_0, t) + N_0^y \gamma_i(N_0^{-y} e^{yt} \kappa_i(N_0 e^{-t}, 0)) \\
&= y \kappa_i(N_0, t) + \tilde{\beta}_i(e^{yt} \kappa_i(N_0 e^{-t}, 0); N_0) \\
&= y \kappa_i(N_0, t) + \tilde{\beta}_i(\kappa_i(N_0, t); N_0) \\
&= \beta_i(\kappa(N_0, t); N_0) \, .
\end{aligned}
\tag{B.10}
$$

C Some details of the TCSA algorithm

In order to calculate the matrix elements of the perturbations one needs to know the functional form of the 3pt function of primary fields on the upper half plane. If the perturbing operator is chiral it is simply

$$\langle A | \phi_h(z) | B \rangle = C \, z^{h_A - h - h_B} \, . \tag{C.1}$$

If the perturbation is non-chiral then the correlation function is more complicated, but if the states A or B belong to the representation $(1, 2)$ or $(2, 1)$ the null vector equations can be used to deduce the form of the correlator.

The equation in the model $M(p, q)$ for B is

$$\langle A | \phi(z, \bar{z})(L_{-1}^2 - t L_{-2}) | B \rangle = 0 \tag{C.2}$$

where $t = p/q$ if $B = \phi_{1,2}$ and $t = q/p$ if $B = \phi_{2,1}$. Commuting the L_n's past ϕ, changing to polar coordinates (r, θ) and using

$$(h_A - h_B)\langle A | \phi_{h, \bar{h}}(r, \theta) | B \rangle = \langle A | [L_0, \phi_{h, \bar{h}}(r, \theta)] | B \rangle = \left(h + \bar{h} + r \frac{\partial}{\partial r} \right) \langle A | \phi(r, \theta) | B \rangle \quad \text{(C.3)}$$

one arrives at the second order differential equation

$$
\Big[\sin^2 \theta \, \partial_\theta^2 + (1 + \Delta - t) \sin 2\theta \, \partial_\theta + \tag{C.4}
$$
$$
\Delta(\Delta + 1) \cos^2 \theta - \Delta \sin^2 \theta - t(\Delta \cos 2\theta + h \, e^{-2i\theta} + \bar{h} \, e^{2i\theta}) \Big] \langle A | \phi_{h, \bar{h}}(r, \theta) | B \rangle = 0
$$

where $\Delta = h_A - h - \bar{h} - h_B$.

The null vector equation for A reads

$$\langle (L_{-1}^2 - t L_{-2}) A | \phi(z, \bar{z}) | B \rangle = 0 \, . \tag{C.5}$$

With the same steps this can be converted to the equation

$$\left[\sin^2\theta \, \partial_\theta^2 + 2\sin\theta \left((1 + 2h + 2\bar{h} - t - \Delta)\cos\theta + 2i(h - \bar{h})\sin\theta \right) \partial_\theta + \right.$$
$$e^{2i\theta} \left(4h^2 - h(3t + 2\Delta - 2) \right) + e^{-2i\theta} \left(4\bar{h}^2 - \bar{h}(3t + 2\Delta - 2) \right) +$$
$$\left. \frac{1}{2}\Delta(\Delta + 2t - 2)\cos(2\theta) + \frac{1}{2}(4h - \Delta)(4\bar{h} - \Delta) \right] \langle A|\phi_{h,\bar{h}}(r,\theta)|B\rangle = 0. \qquad \text{(C.6)}$$

If it is not true that $h_A = h_B$ *and* $h = \bar{h}$ at the same time the equations (C.4) and (C.6) can be combined to obtain a first order equation. In case $h_A = h_B$ and $h \neq \bar{h}$ one gets

$$\left[\partial_\theta + (1 + h + \bar{h} - 2t)\cot\theta + i(h - \bar{h}) \right] \langle A|\phi_{h,\bar{h}}(r,\theta)|B\rangle = 0 \qquad \text{(C.7)}$$

having the solution

$$\langle A|\phi_{h,\bar{h}}(r,\theta)|B\rangle = C \, r^{-h-\bar{h}} e^{-i(h-\bar{h})\theta} \sin\theta^{-1+2t-h-\bar{h}} = \qquad \text{(C.8)}$$
$$= \tilde{C} z^{(1-2t-h+\bar{h})/2} \bar{z}^{(1-2t+h-\bar{h})/2} (z - \bar{z})^{-1+2t-h-\bar{h}}. \qquad \text{(C.9)}$$

The matrix elements of the perturbation in the basis (5.3) can be calculated using the relations

$$\langle L_{-n}A|\phi(z,\bar{z})|B\rangle = \sum_{k=-1}^{n} \binom{n+1}{k+1} \left(z^{n-k}\langle A|L_k\phi(z,\bar{z})|B\rangle + \bar{z}^{n-k}\langle A|\bar{L}_k\phi(z,\bar{z})|B\rangle \right) +$$
$$\langle A|\phi(z,\bar{z})|L_n B\rangle, \qquad \text{(C.10)}$$
$$\langle A|\phi(z,\bar{z})|L_{-n}B\rangle = -\sum_{k=-1}^{\infty} \binom{-n+1}{k+1} \left(z^{-n-k}\langle A|L_k\phi(z,\bar{z})|B\rangle + \bar{z}^{-n-k}\langle A|\bar{L}_k\phi(z,\bar{z})|B\rangle \right) +$$
$$\langle L_n A|\phi(z,\bar{z})|B\rangle. \qquad \text{(C.11)}$$

For ϕ left chiral the terms containing $\bar{z}$ are not present. Applying these relations iteratively every matrix element becomes a sum of correlators of the form

$$\langle A|L_{-1}^k \bar{L}_{-1}^l \phi(z,\bar{z})|B\rangle \qquad\qquad A, B \text{ primary.} \qquad \text{(C.12)}$$

The action of L_{-1}'s translates to derivatives of (C.1) or (C.9) with respect to z and $\bar{z}$.

D Position invariance of the spectrum for a chirally perturbed defect

Let $H(\theta)$ be the Hamiltonian in (5.2) for the perturbation by a single chiral field $\phi_{h,0}$,

$$H(\theta) = H_0 + H_I(\theta) \quad \text{where} \quad H_0 = \frac{\pi}{R}\left(L_0 - \frac{c}{24} \right), \quad H_I(\theta) = \lambda_l \left(\frac{\pi}{R} \right)^h e^{ih\theta} \phi_{h,0}(e^{i\theta}). \qquad \text{(D.1)}$$

We will show that

$$H(\theta) = e^{i\theta L_0} H(0) e^{-i\theta L_0} \qquad \text{(D.2)}$$

by verifying it on matrix elements. Clearly, $e^{i\theta L_0} H_0 e^{-i\theta L_0} = H_0$, so that it is enough to show $H_I(\theta) = e^{i\theta L_0} H_I(0) e^{-i\theta L_0}$. On the one hand, from (5.8) we have, in the notation of that section,

$$\langle v_i|H_I(\theta)|v_j\rangle = \lambda_l \left(\frac{\pi}{R} \right)^h e^{ih\theta} C \, e^{i\theta(\Delta_i - h - \Delta_j)}, \qquad \text{(D.3)}$$

where the constant C is given by $C = \langle v_i | \phi_h(1) | v_j \rangle$. On the other hand,

$$\langle v_i | e^{i\theta L_0} H_I(0) e^{-i\theta L_0} | v_j \rangle = e^{i\theta(\Delta_i - \Delta_j)} \langle v_i | H_I(0) | v_j \rangle = e^{i\theta(\Delta_i - \Delta_j)} \lambda_l \left(\frac{\pi}{R} \right)^h \langle v_i | \phi_{h,0}(1) | v_j \rangle \tag{D.4}$$

These two expressions coincide. We see that $H(\theta)$ and $H(0)$ are related by a similarity transformation, and hence have the same spectrum. For the application to TCSA it is important to note that the operator $e^{i\theta L_0}$ commutes with the projection P_N to the truncated Hilbert space, so that also

$$P_N H(\theta) P_N = e^{i\theta L_0} P_N H(0) P_N e^{-i\theta L_0} . \tag{D.5}$$

Thus even in TCSA, the truncated Hamiltonians for different positions θ of the chirally perturbed defect on the strip have *exactly* the same spectrum. For a perturbation by an anti-chiral field $\phi_{0,h}$, the argument is the same, except that the similarity transformation in this case is $H(\theta) = e^{-i\theta L_0} H(0) e^{i\theta L_0}$.

References

[1] I. Affleck and A.W.W. Ludwig, *Universal noninteger "ground state degeneracy" in critical quantum systems*, *Phys. Rev. Lett.* **67** (1991) 161 [SPIRES].

[2] C. Bachas, J. de Boer, R. Dijkgraaf and H. Ooguri, *Permeable conformal walls and holography*, *JHEP* **06** (2002) 027 [hep-th/0111210] [SPIRES].

[3] C. Bachas, *On the Symmetries of Classical String Theory*, published in *Quantum Mechanics of Fundamental Systems: The Quest for Beauty and Simplicity*, J. Zanelli and M. Henneaux eds., Springer, New York U.S.A. (2009), pg. 1–10, http://dx.doi.org/10.1007/978-0-387-87499-9 [arXiv:0808.2777] [SPIRES].

[4] C. Bachas and I. Brunner, *Fusion of conformal interfaces*, *JHEP* **02** (2008) 085 [arXiv:0712.0076] [SPIRES].

[5] C. Bachas and M. Gaberdiel, *Loop operators and the Kondo problem*, *JHEP* **11** (2004) 065 [hep-th/0411067] [SPIRES].

[6] I. Brunner and D. Roggenkamp, *B-type defects in Landau-Ginzburg models*, *JHEP* **08** (2007) 093 [arXiv:0707.0922] [SPIRES].

[7] I. Brunner and D. Roggenkamp, *Defects and Bulk Perturbations of Boundary Landau-Ginzburg Orbifolds*, *JHEP* **04** (2008) 001 [arXiv:0712.0188] [SPIRES].

[8] J.L. Cardy, *Boundary Conditions, Fusion Rules and the Verlinde Formula*, *Nucl. Phys.* **B 324** (1989) 581 [SPIRES].

[9] P. Dorey, A. Pocklington, R. Tateo and G. Watts, *TBA and TCSA with boundaries and excited states*, *Nucl. Phys.* **B 525** (1998) 641 [hep-th/9712197] [SPIRES].

[10] G. Feverati, K. Graham, P.A. Pearce, G.Z. Toth and G. Watts, *A renormalisation group for TCSA*, *J. Stat. Mech.* (2008) P03011 [hep-th/0612203] [SPIRES].

[11] P. Fendley, M.P.A. Fisher and C. Nayak, *Boundary Conformal Field Theory and Tunneling of Edge Quasiparticles in non-Abelian Topological States*, *Annals Phys.* **324** (2009) 1547 [arXiv:0902.0998] [SPIRES].

[12] S. Fredenhagen and M.R. Gaberdiel, *Generalised $N = 2$ permutation branes*, *JHEP* **11** (2006) 041 [hep-th/0607095] [SPIRES].

[13] S. Fredenhagen, M.R. Gaberdiel and C. Schmidt-Colinet, *Bulk flows in Virasoro minimal models with boundaries*, arXiv:0907.2560 [SPIRES].

[14] S. Fredenhagen and T. Quella, *Generalised permutation branes*, *JHEP* **11** (2005) 004 [hep-th/0509153] [SPIRES].

[15] D. Friedan and A. Konechny, *On the boundary entropy of one-dimensional quantum systems at low temperature*, *Phys. Rev. Lett.* **93** (2004) 030402 [hep-th/0312197] [SPIRES].

[16] J. Fröhlich, J. Fuchs, I. Runkel and C. Schweigert, *Kramers-Wannier duality from conformal defects*, *Phys. Rev. Lett.* **93** (2004) 070601 [cond-mat/0404051] [SPIRES].

[17] J. Fröhlich, J. Fuchs, I. Runkel and C. Schweigert, *Duality and defects in rational conformal field theory*, *Nucl. Phys.* **B 763** (2007) 354 [hep-th/0607247] [SPIRES].

[18] J. Fuchs, I. Runkel and C. Schweigert, *TFT construction of RCFT correlators. I: Partition functions*, *Nucl. Phys.* **B 646** (2002) 353 [hep-th/0204148] [SPIRES].

[19] J. Fuchs, M.R. Gaberdiel, I. Runkel and C. Schweigert, *Topological defects for the free boson CFT*, *J. Phys.* **A 40** (2007) 11403 [arXiv:0705.3129] [SPIRES].

[20] K. Graham, *On perturbations of unitary minimal models by boundary condition changing operators*, *JHEP* **03** (2002) 028 [hep-th/0111205] [SPIRES].

[21] K. Graham, I. Runkel and G.M.T. Watts, *Renormalisation group flows of boundary theories*, in proceedings of *4th Annual European TMR Conference on Integrability Nonperturbative Effects and Symmetry in Quantum Field Theory*, Paris France, September 7–13 2000, hep-th/0010082 [SPIRES].

[22] K. Graham and G.M.T. Watts, *Defect lines and boundary flows*, *JHEP* **04** (2004) 019 [hep-th/0306167] [SPIRES].

[23] F. Lesage, H. Saleur and P. Simonetti, *Boundary flows in minimal models*, *Phys. Lett.* **B 427** (1998) 85 [hep-th/9802061] [SPIRES].

[24] M. Oshikawa and I. Affleck, *Boundary conformal field theory approach to the critical two-dimensional Ising model with a defect line*, *Nucl. Phys.* **B 495** (1997) 533 [cond-mat/9612187] [SPIRES].

[25] V.B. Petkova and J.B. Zuber, *Generalised twisted partition functions*, *Phys. Lett.* **B 504** (2001) 157 [hep-th/0011021] [SPIRES].

[26] T. Quella, I. Runkel and G.M.T. Watts, *Reflection and Transmission for Conformal Defects*, *JHEP* **04** (2007) 095 [hep-th/0611296] [SPIRES].

[27] T. Quella and V. Schomerus, *Symmetry breaking boundary states and defect lines*, *JHEP* **06** (2002) 028 [hep-th/0203161] [SPIRES].

[28] A. Recknagel, D. Roggenkamp and V. Schomerus, *On relevant boundary perturbations of unitary minimal models*, *Nucl. Phys.* **B 588** (2000) 552 [hep-th/0003110] [SPIRES].

[29] I. Runkel, *Perturbed Defects and T-Systems in Conformal Field Theory*, *J. Phys.* **A 41** (2008) 105401 [arXiv:0711.0102] [SPIRES].

[30] E. Wong and I. Affleck, *Tunneling in quantum wires: A Boundary conformal field theory approach*, *Nucl. Phys.* **B 417** (1994) 403 [SPIRES].

[31] V.P. Yurov and A.B. Zamolodchikov, *Truncated conformal space approach to scaling Lee-Yang model*, *Int. J. Mod. Phys.* **A 5** (1990) 3221 [SPIRES].